

GL04049

Electrical Methods  
in  
Mining Geophysics

by

\*Gerald W. Hohmann  
and  
\*Stanley H. Ward

\*Geology and Geophysics Department  
University of Utah, Salt Lake City, UT 84112

## ABSTRACT

Electrical methods of geophysics are fundamental in mineral exploration, because they can directly detect and delineate conductive sulfide minerals. Electromagnetic (EM) methods are used in exploring for massive sulfides due to their high conductivity. The introduction of induced polarization (IP) in the 1950's represented a major advance in mining geophysics by making possible the direct detection of disseminated sulfides.

Both IP and EM have benefitted from research directed at achieving greater resolution and greater depth of exploration. The major advances in IP have been: digital instrumentation for greater accuracy, techniques for eliminating or reducing EM coupling effects, and numerical modeling techniques for improved interpretation. In EM, numerical and physical scaled modeling have led to the recognition of the importance of current channeling and to improved interpretation aids. Broadband, multi-coil measurements provide better conductor discrimination in both ground and airborne applications. Time domain EM is assuming greater importance due to its interpretation simplicity and its capabilities for deep exploration.

## Introduction

### *Basic Principles*

All electrical geophysical methods involve the measurement of an *impedance*, with subsequent interpretation in terms of the subsurface electrical properties and, in turn, the subsurface geology. Basically an impedance is the ratio of the response (output) to the excitation (input). In the resistivity and induced polarization (IP) methods the input is a current injected into the ground between two electrodes, while the output is a voltage measured between two other electrodes. In the electromagnetic (EM) method the input usually is a current through a coil of wire, and the output is the voltage induced in another coil of wire.

In *frequency domain* impedance measurements, the input current is a sine wave with frequency  $f$  and period  $T=1/f$ . The output also is a sine wave, as shown in Figure 1; its amplitude ( $A$ ) and phase ( $\phi$ ) depend upon electrical properties of the earth. In general, the output is delayed by  $\phi \times T/2\pi$  seconds relative to the transmitted waveform. Often it is convenient to decompose the output wave into *in-phase* (real) and *quadrature* (imaginary) components, as shown in Figure 1. If we denote their peak amplitudes as  $V_R$  and  $V_I$ , respectively, then the amplitude and phase of the output waveform are given by

$$A = \sqrt{V_R^2 + V_I^2} ,$$

and

$$\phi = \text{Arctan} \left( \frac{V_I}{V_R} \right) .$$

Impedance also can be measured in the *time domain* in which case the current is periodically turned on and off. As shown in Figure 2, the output is the voltage measured at various times when the transmitter current is off. Note that the input again is periodic, because measurements must be made for each of several periods and then added together, or stacked, to eliminate noise. Time and frequency domain measurements are directly related through the Fourier transform, and in that sense, are equivalent. However, in practice, each system has certain advantages and disadvantages.

There are three basic modes of operation for any electrical method: (1) *sounding*, (2) *profiling* and (3) *sounding-profiling*. In sounding, the transmitter-receiver separation is changed, or the frequency is changed, and the results are interpreted in terms of a layered earth. Because the earth usually is not layered in mineral prospecting, sounding has little application. In profiling, the transmitter or receiver, or both, are moved along the earth to detect anomalies. The most useful method is a combination of sounding and profiling which delineates both lateral and vertical variations.

Electrical methods have become more useful in recent years through advances in both instrumentation and interpretation. Modern field instruments are based on micro-computers. Processing the signals digitally greatly increases the accuracy and, in fact, makes possible new types of measurements. Further, data reduction in the field facilitates more reliable results and more cost-effective surveys.

#### *Electrical properties of rocks*

Crustal rocks conduct electricity primarily via the movement of ions through pore water, although semiconduction in minerals such as sulfides and

graphite sometimes contributes significantly. An electrical current,  $I$ , is a flow of charge, measured by the rate at which charge passes through a surface. The current density,  $\vec{J}$ , is a vector having the direction of the flow of positive charge and a magnitude equal to the current per unit area through a surface normal to the current flow. Ohm's law,

$$\vec{J} = \sigma \vec{E}$$

relates the current density  $\vec{J}$  and electric field  $\vec{E}$  through the *conductivity*  $\sigma$  which, basically, is a measure of the ability of rock to conduct electricity. Resistivity,  $\rho$ , is the reciprocal of conductivity, ; it provides a measure of resistance to current flow. In the MKS system, the unit of  $\rho$  is ohm-meter ( $\Omega\text{-m}$ ), while the unit of  $\sigma$  is mho/meter ( $\mathcal{U}/\text{m}$ ).

In general, the resistivity of a rock varies with frequency and is complex, being represented by its real and imaginary parts ( $\rho = \rho' - i\rho''$ ) or more commonly by its amplitude and phase ( $\rho = |\rho| e^{i\phi}$ ). The phase  $\phi$  is usually measured in milliradians (mrad). The resulting frequency-dependent, complex impedance measured with an electrode array is said to be due to *induced polarization* (IP). In time-domain measurements the voltage decays with time after current shut-off rather than going to zero instantly. Figure 2 illustrates this decay. Hence the current induces a polarization in the rock. A rock that exhibits an IP response is termed polarizable.

Induced polarization is due to the accumulation of charge and the generation of diffusion gradients (1) where the ionic conduction in pore water changes to semiconduction in metallic minerals and (2) where exchange cations, excess positive ions often associated with clays, alter the relative currents carried by the positive and negative ions. The former is called *interfacial* or *electrode polarization* and the latter is called *membrane polarization*.

## *Applications*

The introduction of IP in the 1950's represented a major advance in mining geophysics. For the first time it was possible to detect disseminated sulfides directly, and in concentrations less than 5 or 6 percent by weight. Such low percentages of sulfides do not appreciably alter the amplitude of the resistivity  $\rho$  in view of the large variation in  $\rho$  just due to porosity and salinity changes, but they do produce the induced polarization effect.

EM methods respond only to large changes in  $\rho$ . Hence their primary domain is the detection of massive sulfides, which are highly conductive, at least when the sulfides have been remobilized and interconnected as in Precambrian rocks. Because grounded electrodes are not required, EM surveys generally are less expensive per unit area than IP surveys. Furthermore, they can be carried out from the air. Many massive sulfide ore bodies have been found by airborne EM since its introduction in the early 1950's.

## *Interpretation*

Interpretation of data is accomplished by estimating the parameters of simplified models of the earth. The earth is too complex for its electrical response to be evaluated exactly, but the simplified model, if it is close to reality, achieves the economic goal of identifying a target for drilling.

The three basic types of simple interpretation models are illustrated in Figure 3: one dimensional (1D or layered); two dimensional (2D, body infinitely long in one direction); and three dimensional (3D). Resistivity is denoted by  $\rho$  and IP response by  $\phi$ . Models can be made more complex by including more layers in the 1D case and more bodies in the 2D and 3D cases. Solutions for layered models have been available for many years; they are *analytical*, consisting of integrals or summations. Evaluating the response of a 2D or 3D model is much more difficult, requiring *numerical* solutions which

have become possible only in the last ten years with the availability of large computers. Such solutions are achieved by approximating the relevant differential or integral equation and inverting a large matrix.

There are four basic methods of interpreting data: 1) intuition, 2) comparison with simple numerical or scaled physical models, 3) trial-and-error data fitting with complex numerical models, and 4) inversion. Rudimentary interpretation by intuition is not sufficient for the subtle signatures of the ore deposits that remain to be found. Catalogs of simple models are essential for proper survey design, for rough field interpretations, and for insight into more sophisticated interpretation schemes. Trial and error data fitting with complex models, the current state of the art, is very useful, but time consuming.

Inversion, i.e. programming a computer to calculate a model based on the data, has the potential for significantly enhancing the science of interpretation. The optimum model and the range of acceptable models can both be found via inversion. It is doubtful, however, that strictly automated inversion can be applied to complex earths because of a) the large range of acceptable models which will satisfy the field data, b) the presence of geological noise, and c) the large amount of computer time involved. Probably some combination of trial-and-error fitting and inversion will be found to be optimum.

## Resistivity and Induced Polarization Methods

### *Basic principles*

The resistivity and induced polarization (IP) methods are based on the response of earth materials to the flow of current at low frequencies. The D.C. resistivity method is based on potential theory which requires *direct*

current, but noise and measurement problems quickly lead to the use of *alternating currents* (A.C.) of low frequency, so that the resistivity method now employs A.C. exclusively. The induced polarization method, on the other hand, requires the use of alternating current, because it is based on changes in resistivity as a function of frequency. As the frequency increases to some critical frequency determined by the resistivity of the materials and the scale size of the measurement, *electromagnetic coupling* between transmitting and receiving circuits violates potential theory so that electromagnetic theory is required.

Measurements are made with a four-electrode array consisting of two current and two potential electrodes. Resistivity data always are recorded along with IP to aid in interpretation. For a homogeneous earth the resistivity is given by

$$\rho = K \frac{\Delta V}{I}$$

where  $I$  is the current,  $\Delta V$  is the measured potential difference, and  $K$  is a geometric factor that depends on the electrode configuration. When the ground is not homogeneous, the voltage and current data are reduced in the same fashion, but the resistivity is called the *apparent resistivity*. It is the resistivity of a homogeneous earth that would produce the same measurement.

The IP parameters measured depend on whether the system makes use of a time domain or frequency domain waveform (Figures 1 and 2). For time domain measurements, the maximum value of the voltage during the on cycle, along with the current, can be used to calculate the apparent resistivity. The transient during the off cycle contains the basic time domain IP information. This transient is specified by its normalized value just after the current is turned off and by the form and rate of decay. For frequency domain



measurements the basic data are the magnitude and phase angle of the measured voltage as functions of frequency, from which the amplitude and phase of the apparent resistivity are calculated.

Older analogue time domain receivers integrate one or several intervals under the decay curve, at sampling times ranging from around 0.05 sec to 2.0 sec. after current shut-off. When the integrated voltage is normalized by the primary voltage ( $V_0$ ) and the integration time ( $\Delta t$ ), the unit of the measurement is given as mV/V (millivolts per volt) and is called the *chargeability* (M). Another definition of chargeability, the Newmont Standard, does not normalize by the integration time; the units are (mV-sec)/V or m-sec. Since the equivalent integration time of the Newmont Standard is one sec, normalization by the integration time does not change the numerical value of the chargeability. The Newmont Standard is often written as M331, which refers to a standard pulsed square wave of 3 sec on, 3 sec off, and an integration time of 1 sec. Often measurements are made using different pulse lengths and integration times which are then reduced to an equivalent M331 using various model-dependent normalization factors (Sumner, 1976).

Analogue frequency domain receivers often use two to five frequencies, and many have no current waveform reference, so that phase information is lost. The basic data are then the magnitudes of the apparent resistivity,  $\rho_1$  and  $\rho_2$  at two frequencies,  $f_1$  and  $f_2$ , which can be used to calculate percent frequency effect (PFE),

$$PFE = 100 \frac{\rho_1 - \rho_2}{\rho_1} ,$$

where,  $\rho_1$  is the resistivity at the lower frequency.

Modern digital receivers sample the waveform at discrete points in time and store the samples as numbers in the computer memory. Manipulation of the

data stored in memory is under program control and, in principle, either time- or frequency-domain processing can be done. To increase the ratio of signal to noise, multiple cycles are stored and averaged, or stacked, in the memory. Phase information is obtained by using a pair of very accurate, synchronized oscillators at the receiver and transmitter or by using a cable link between the receiver and transmitter.

For the Newmont Standard of chargeability, time domain and frequency domain IP units are related by:

$$M \approx \phi(\text{mrad}) \approx 7\text{PFE/decade of frequency}$$

Normally IP effects produce a positive PFE, a phase lag (negative phase angle) and a secondary decay voltage with the same sign as the primary (M positive); by convention these are referred to as positive IP effects. Negative IP response (positive phase angle) can be caused by geometric effects with normally polarizable materials and by inductive coupling. Precise measurements are required in IP surveys; even a large IP response of 50 mrad is a phase shift of only 3 degrees.

#### *Problems*

Because resistivity is less important than IP in mineral exploration, we will concentrate on problems with IP. Since its inception, IP has been plagued by a number of problems; some have been overcome, some will benefit from future research, and some represent fundamental limitations. In the following we discuss the existing major problems.

*Overburden masking:* Conductive overburden, generally in the form of porous alluvium or weathered bedrock, prevents current from penetrating to sulfides in the more resistive bedrock. Hence the sulfides influence the measurements less than they would if the overburden were absent. Figure 4 illustrates the effect of conductive overburden on the theoretical IP

response, in mrad, of a 2D body. These results are for the dipole-dipole electrode array and are plotted in *pseudosection* form (Sumner, 1976). Values are plotted at the intersection of 45-degree diagonal lines leading downward from the transmitter and receiver dipoles. A pseudosection is merely a convenient way of displaying data from many transmitter-receiver dipole pairs, and in no way should it be taken as a true section of the earth.

In all theoretical pseudosections to follow, the contours are shown as a percentage of the intrinsic response of the body and therefore are labeled  $B_2(\%)$ . The upper pseudosection in Figure 4 shows the IP response  $B_2(\%)$  without overburden, while the lower one shows the IP response  $B_2(\%)$  with overburden 1 dipole length in thickness and 10 times as conductive as the bedrock. In this realistic example, overburden reduces the IP response by roughly a factor of 3.

For surface electrode arrays, conductive overburden represents a fundamental limitation. However, one way of combatting it is to force current into the bedrock by placing an electrode in a drill hole. In another approach, Seigel (1974) claims that measuring the magnetic field of a polarizable body is superior to measuring the electric field, as in conventional IP, in areas of conductive overburden.

*Electromagnetic coupling:* Electromagnetic (EM) coupling presents a serious problem for IP surveys, particularly when large electrode separations are used in areas of low resistivity. The EM eddy currents induced in the ground by current in the transmitting circuit vary with frequency, and their effects are similar to those of sulfide mineralization.

The first step in combatting EM coupling is to use an appropriate electrode array. Arrays such as the Schlumberger and Wenner (Telford et al., 1976), where measurements are made between widely spaced current electrodes,

generate large EM coupling and must not be used except where resistivities are high. If a long current line is necessary to increase the signal in low-resistivity terrain, measurements must be made perpendicular to the current wire near one of the electrodes, as in the three-array or the perpendicular pole-dipole array. If the earth is homogeneous, there is no EM coupling with a perpendicular array. But lateral or vertical resistivity changes can produce large, and sometimes negative, EM coupling. The commonly used in-line dipole-dipole array offers both high earth resolution and lower EM coupling, at the expense of low receiver voltage levels.

Even if an optimum array is used, however, EM coupling poses a serious problem. Figure 5, for example, shows the theoretical EM coupling phase over a 2000 ft (610 m) wide by 3000 ft (915 m) depth extent by 6000 ft (1830 m) long prism at a depth of 1000 ft (305 m). Its resistivity is 1  $\Omega$ -m, and the background resistivity is 100  $\Omega$ -m. The dipole length is 1000 ft (305 m). Results are shown for three frequencies: 1.0 Hz, 0.5 Hz, and 0.1 Hz. For comparison, EM coupling values for a homogeneous half-space of resistivity 100  $\Omega$ -m are shown at the right, these are the values of EM coupling that would be observed over a strictly homogeneous earth (i.e. homogeneous half-space). EM coupling is greater than the half-space coupling when the transmitter and receiver straddle the body at large separations. However, there are areas in the pseudosection where EM coupling over the prism is less than half-space coupling. In fact, negative EM coupling often is seen in field data taken over very conductive bodies.

The level of EM coupling shown in Figure 5 is unacceptable, even at 0.1 Hz, for an IP anomaly of interest may be as low as 10 mrad or less. Furthermore, background resistivities below 100  $\Omega$ -m are common and would result in much greater phase angles. Hence, some means must be devised to

eliminate EM coupling. The EM effects would decrease at lower frequencies, but due to increasing natural electric fields, reliable measurements often cannot be made below 0.1 Hz. Time domain practitioners reduce the problem by using high currents and large, perpendicular arrays, and by allowing a large time interval between current shut-off and voltage measurement. This technique usually is successful because the EM coupling decays more rapidly than the IP response.

However, in situ IP measurements with short electrode spacings show that the IP phenomenon persists to frequencies below .01 Hz, and that in most cases the IP phase angle is approximately constant between .01 Hz and 10 Hz (Van Voorhis et al., 1973). Based on these results, Van Voorhis devised a simple, effective technique for eliminating EM coupling; a similar technique was published by Hall of (1974). The method is illustrated in Figure 6. The phase is the sum of two components: (1) caused by IP, which is constant with frequency and persists to very low frequencies; and (2) due to EM coupling, which varies with frequency and is negligible at very low frequencies. By fitting the IP data to a polynomial and extrapolating to zero frequency, as shown in Figure 6, EM coupling usually is eliminated. Generally, a second-degree polynomial is required; linear extrapolation is not sufficient.

Techniques for removing EM coupling over a broad frequency range have been proposed by Wynn and Zonge (1975) and Pelton et al. (1978).

*Natural fields:* Natural electric and magnetic fields below 1 Hz are due mainly to the interaction of fields and particles from the sun with the earth's magnetic field, and hence their magnitude depends on solar activity. Above 1 Hz they are primarily due to worldwide thunderstorms. As Figure 18 shows, their amplitude increases rapidly with decreasing frequency below 1 Hz and effectively prevents IP measurements below about 0.03 Hz. Since EM

coupling is too high above 3 Hz, IP measurements with large arrays are limited to the range 0.03 to 3 Hz. Even in that range, coherent detection and digital high-pass filtering are required to make accurate measurements because of the natural field noise. Stacking, i.e. adding successive transients, is necessary to reduce noise in time domain measurements, but noise rejection is not as good as for coherent detection in the frequency domain.

Another promising method, suggested by Halverson (1977), utilizes multiple receiver dipoles to reduce electric field noise. Natural fields are more uniform than the artificial fields of interest, so they can be cancelled by making simultaneous measurements at a location that is not affected by the transmitter current.

*Geological noise:* Any response from a body or zone that is not of economic interest, and that interferes with the target response, is termed geological noise. Geological noise always is high in resistivity surveys because of the large variations of resistivity due to changes in porosity and water saturation. In effect, it prevents resistivity from being much more than an accessory to IP in most mineral exploration.

However, magnetometric resistivity (MMR) is a promising new method designed to delineate resistivity boundaries beneath conductive overburden. In this resistivity method the magnetic field rather than the electric field is measured in the vicinity of grounded electrodes. Because it is an integral over a volume distribution of current, the magnetic field is much less distorted than the electric field by surficial inhomogeneities. Edwards and Howell (1976) show a field example of delineation of a fault beneath a considerable thickness of variably conductive overburden using MMR; standard resistivity methods would have been useless in this instance due to large geological noise from the overburden.

Geological noise in IP surveys is due to uneconomic sulfide mineralization, clays and zeolites, carbonaceous sedimentary rocks, magnetite, and possibly other sources. There are some indications that it may be possible to distinguish among clay, sulfide, and graphite responses on the basis of their spectral characteristics using broad-band measurements with short electrode spacings. Basically, clay response has a rapid decay or short time constant, while very conductive graphite has a slow decay or large time constant.

In the only definitive published study of IP spectra, Pelton et al. (1978) measured in situ IP response in several types of mineralization over a broad frequency range using short electrode spacings. Laboratory measurements on core are not very useful for this purpose; results are highly variable due to the small sample size. Typical phase spectra from porphyry copper, massive sulfide, and graphite deposits are shown in Figure 7. The most distinguishing characteristic is the position of the peak of the phase response. Phase peaks at lower frequencies are due to greater interconnection of metallic particles. Thus the possibility for mineral discrimination is based on the texture rather than mineralogy. However, it is doubtful that this discrimination can be achieved in typical field surveys, where large electrode spacings lead to high EM coupling and averaging of many kinds of IP responses, and where natural field noise limits the lowest frequency to about 0.03 Hz. Because geological noise is so detrimental in IP surveys, much current research is concentrated on this problem.

*Culture:* Grounded structures such as fences, powerlines, and pipelines redistribute current from the IP transmitter so that part of the current flows through the cultural feature. The complex grounding impedance causes an IP response that is virtually indistinguishable from a sulfide response. In a

definitive analysis of the problem, Nelson (1977) finds that the only certain means of eliminating such spurious IP responses is to keep IP transmitting and receiving lines away from grounded structures.

Cultural features also can introduce noise into IP measurements by providing a path for various interfering signals. Of course strong noise voltages are present in the vicinity of powerlines, requiring filtering at the front end of the receiver. Pipelines, furthermore, often carry electrical current for cathodic protection and this current is a source of noise.

*Topography:* Much mineral exploration is done in mountainous terrain where topography can produce spurious resistivity anomalies. In a recent study, Fox et al. (1980) have systematically analyzed the effects of topography for the dipole-dipole array using a 2D numerical solution. Figure 8, for example, shows the apparent resistivity anomaly produced by a valley with 30 degree slopes. The pseudosection is characterized by a central zone of low apparent resistivity flanked by zones of high apparent resistivity. The low is most pronounced when the transmitter and receiver dipoles are on extreme opposite sides of the valley. This example shows that a valley can produce a large, spurious low in resistivity which could easily be misinterpreted as evidence for a buried conductor. Similarly, a hill can produce an apparent resistivity high.

Because IP is a normalized measurement, current focusing and dispersion produced by an irregular terrain surface do not significantly affect IP data. Thus if the earth were homogeneous and polarizable, irregular terrain would produce no significant spurious IP response. However, second-order topographic effects in IP surveys are introduced by variations in distances between surface electrodes and a polarizable body relative to a flat earth.

The significance of an IP anomaly often depends upon its associated



resistivity anomaly. For example, an IP anomaly due to sulfide mineralization may have a corresponding resistivity low associated with hydrothermally altered host rock. The resistivity high caused by a ridge could mask a zone of low resistivity associated with an IP anomaly, suggesting a source in fresh, rather than altered, host rock. A moderately anomalous IP response associated with the resistivity low caused by a valley could be interpreted as positive evidence for significant sulfide mineralization when in reality the IP anomaly would be due to high inherent IP response in a rock of high resistivity.

In general, topographic effects are important where slope angles are 10 degrees or more for slope lengths of one dipole or more. The solution to the problem is to include the topographic surface in numerical models used for interpretation.

#### *Interpretation*

*Models:* One dimensional interpretation, i.e. use of layered earth models, has reached an advanced state. Efficient computer inversion algorithms produce reliable solutions, and, furthermore, they provide estimates of the attainable resolution. Unfortunately, such techniques only occasionally are useful in mineral exploration, where the target usually has finite lateral extent.

Before about 1970, resistivity/IP interpretation in mineral exploration was rudimentary and unsatisfactory because of a lack of forward solutions. Since then, however, computer programs that calculate the responses of assumed 2D and 3D models have been developed. It is now possible to compute catalogs of simple, realistic models for comparison with field data. Hohmann (1977) shows examples from such a catalog. More detailed interpretation can be carried out by trial-and-error matching of data with theoretical responses for

complex models. However, practical inversion techniques for 2D and 3D models do not yet exist, although they are the subject of much research.

We show a few results of simple 3D models to illustrate some important points. We consider only IP responses and only the dipole-dipole array because of their importance in mineral exploration. They were computed using the integral equation technique described by Hohmann (1975). IP responses are given as a percentage of the intrinsic response in the body  $B_2(\%)$ , so that they apply to any IP parameter such as phase, PFE, or chargeability. Coggon (1973) compares the commonly used electrode arrays, based on 2D numerical modeling results.

*Electric field patterns in the earth:* Looking at IP in terms of the mathematical modeling technique provides an intuition for IP behavior. The measured potential is the sum of the primary and secondary potentials. The former is what would be measured over a homogeneous earth of resistivity  $\rho_1$ , while the latter represents the contribution from the inhomogeneity. The secondary potential consists of in-phase and quadrature components; they originate at polarization dipoles distributed throughout the body, or equivalently, at surface charges on the body. The quadrature dipoles, as well as the in-phase dipoles for a conductive body, are oriented, roughly, in the same direction as the incident field. For a resistive body, the in-phase dipoles are oriented in the opposite direction.

To illustrate, Figure 9 shows the quadrature (IP) current pattern in a cross section of the earth through the center of a body which is 1 unit wide (W), 1 unit in depth extent (DE) by 5 units long, (L) buried at a depth (D) of 0.5 units. A corresponding pseudosection is shown; the bold numbers correspond to the particular transmitter dipole to which the electric field pattern pertains. The contoured numbers in the cross section are the phase of

the total electric field, i.e., total quadrature field divided by total in-phase field. In this case the in-phase field is the field of a homogeneous earth because there is no resistivity contrast. Because the intrinsic IP response of the body is 100 mrad, the numbers shown are percentages of the intrinsic response, called  $B_2(\%)$ . The solid arrows show the direction of the quadrature field, while the broken arrows show the direction of the in-phase field.

The dipole-dipole array measures the component of electric field along the traverse line. By convention, the IP response is positive when the quadrature, or polarization, and in-phase field are in opposite directions, and negative when they are in the same direction. IP response is negative to the left of the transmitter dipole of Figure 9, and there are two changes in sign to the right. Comparing the pseudosection and the cross-section, we see how negative IP responses arise when both transmitter and receiver are on one side of a body and when they are on opposite sides of a body at large separations. Note the positions of positive and negative surface charges from which the quadrature field originates.

*Depth interpretation:* One of the most important source parameters to determine in exploration is the depth to the top of a polarizable body. Fortunately, dipole-dipole data are very diagnostic. Figure 10 compares the IP responses of a 3D prism at depths of 0.5, 1, and 2 dipole lengths. The prism has dimensions  $W \times L \times DE$  of 1, 2 and 4 dipole lengths; its resistivity is the same as that of the surrounding earth. IP response varies with body depth differently for different points in the pseudosection, therefore, the pattern of the response is important for depth interpretation. In general, deeper bodies give rise to broader, lower-amplitude anomalies.

*Resistivity contrast:* IP response is highly dependent on the ratio of

polarizable body resistivity ( $\rho_2$ ) to host rock resistivity ( $\rho_1$ ). The response peaks at intermediate contrasts and decreases for very resistive and for very conductive bodies. To summarize this behavior, we have plotted in Figure 11 the peak dipole-dipole IP response as a function of resistivity contrast for a sphere of radius one, a 3D body of 2 units W, 4 units DE, and 5 units L, and two 2D bodies. All are at one unit depth.

The response of the sphere in Figure 11 peaks at  $\rho_2/\rho_1 = 0.5$ , and that of the 2 x 4 x 5 body peaks at  $\rho_2/\rho_1 = 0.3$ . However, response curves for 2D bodies are different; they peak at  $\rho_2/\rho_1 < 0.1$ . The position of the peak seems to be controlled by body thickness; the peak occurs at lower values of  $\rho_2/\rho_1$  for thinner bodies. Thus, for example, the IP response of a very conductive (say  $\rho_2/\rho_1 = .02$ ) 3D body is negligible, while that for a 2D body of the same contrast is substantial. Hence, a long massive sulfide body, even though it is very conductive, can produce a large IP anomaly.

Furthermore, those types of models that assume only a volume distribution of polarizable material, do not tell the whole story for very conductive bodies. If they did, there would be no IP response from a grounded pipeline. Nelson (1977) shows that IP effects from grounded conductors, such as pipelines, powerlines, or fences, can be calculated by assuming that the grounding points act as point sources of secondary field. It is necessary to use a similar approach to calculate the IP effect from very conductive massive sulfide or graphite bodies. Most of the IP response probably originates at the surface of the body where current enters and leaves rather than at polarization dipoles throughout the body. IP response from good conductors, then, can be much larger than would be predicted by techniques that model a polarizable volume of material.

*Multiple bodies:* Superposition of IP responses from two or more bodies

frequently leads to misinterpretation. Figure 12 shows how the IP responses of two prisms superpose as they are moved closer together. Each prism is conductive ( $\rho_2/\rho_1 = 0.2$ ), has dimensions 1 x 4 x 5 (W x DE x L), and occurs at depth 1. This case dramatically illustrates the need for sophisticated interpretation of IP anomalies: a pseudosection should not be construed as a cross-section of the earth. Drilling would be unsuccessful if a hole were spotted over the IP high in the pseudosection in the two cases where the bodies are separated. "Bullseye" pseudosection anomalies such as these usually are caused by superposition. When the bodies join, their responses merge into that for a single wide body, as shown in the lower pseudosection of Figure 12.

#### *Applications*

*Deep sulfide mineralization:* One of the main applications of IP is in porphyry copper exploration because it provides a means of directly detecting disseminated sulfides, which do not appreciably affect the resistivity of the host rock. Now that digital receivers can provide very accurate IP data and EM coupling can be minimized by the phase extrapolation technique described above, IP is indispensable in searching for disseminated sulfides beneath post-mineral cover.

Figure 13, an IP line from Kennecott's, Safford, Arizona, porphyry copper deposit shows that sulfides can be detected at great depths beneath overburden of high resistivity. These data were collected in 1969 by G. D. Van Voorhis with the Kennecott Mk 3 phase-measuring IP gear. The overburden in this case consists of 1000 ft (305 m) of post-mineral volcanics plus 500 to 1000 ft (152 to 305 m) of oxidized host rock. The dipole length is 1000 ft (305 m); the sulfide body is detected by electrode separations of 3000 ft (915 m) or more. Accurate data and EM coupling removal are necessary because the IP

response is only about 15 mrad above a general background response of 5 mrad.

*Low resistivity cover:* Figure 14 shows 1000-ft (305 m), dipole-dipole IP phase data taken with the Kennecott Mk 4 unit over the Lakeshore porphyry copper deposit in Arizona. This example illustrates the use of IP in searching for disseminated sulfides beneath alluvium of low resistivity on a pediment adjacent to slightly mineralized outcrop.

The low apparent resistivities on the west end of the line are due to alluvium, while outcropping bedrock produces the high apparent resistivities on the east end of the line. The sulfide body producing the IP response lies at depths on the order of 800 ft (244 m) to the east and 1800 ft (549 m) to the west. Again accurate data and elimination of EM coupling are necessary to define the 15 mrad anomaly in a 3 mrad background. Computer modeling of the data indicates that the drilled sulfides account for the observed anomaly if the sulfide system has a bulk intrinsic response of 60 mrad.

## Electromagnetic Methods

### *Induction and current gathering*

The EM methods of geophysical exploration depend upon the fundamental relationship between electricity and magnetism. An alternating current flowing in a wire at or above the earth's surface will cause an associated *primary* alternating magnetic field to pervade the space adjacent to the wire. If the space is partly or wholly occupied by conducting materials such as rocks and ores, then *secondary* currents will be induced in these conductive materials by the primary field. The secondary currents in the rocks and ores will have associated with them *secondary* alternating magnetic fields. These secondary fields will react with the primary field to produce a *resultant* field. It is expected, then, that the resultant field will contain

information on the geometrical and electrical properties of the distribution of rocks and ores.

Figure 15 portrays a generalized model of the earth in which a massive sulfide body is the object of search for the EM method. An alternating current flows through a *transmitting coil* creating an alternating magnetic field in its vicinity. This latter field, we shall assume for simplicity at the outset, induces alternating currents to flow in the massive sulfide body. These currents will circulate in closed loops only within the massive sulfide body under this assumption as shown by the arrows in Figure 16a. The actual configuration of these circulating currents will be determined by the geometry and location of both the transmitting coil and the massive sulfide body, and by the frequency of the field transmitted.

Let us now make a different assumption; induced currents flow in an assumed homogeneous earth, perhaps as depicted by the arrows in Figure 16b. The configuration of currents in Figure 16b is dictated only by the geometry and location of the transmitting coil and by the frequency of the transmitted field, provided the surface topography is reasonably flat.

In the early days of EM prospecting one customarily attempted to eliminate currents of the type portrayed in Figure 16b and to allow only currents of the type portrayed in Figure 16a. In that manner one could concentrate on the geometrical and electrical information about the massive sulfide body contained in the resultant field. Unfortunately, experience revealed that one could not ignore the currents induced in the host rock (Figure 16b) or, for that matter, currents induced in the other elements of the geoelectric section of the model of Figure 15. In fact, if one discarded the overburden, the weathered layer, the graphitic shear, and the disseminated sulfide halo of Figure 15, he still had to be content with the fact that the

resultant magnetic field reflected the presumably superimposed effects of the two quite different current distributions of Figures 16a and 16b. Could one then still separate the effects of the two? For some time explorationists assumed that they could. Then it was realized that currents induced in a homogeneous half-space as in Figure 16b would be deflected, or *gathered*, into the massive sulfide body and intensified once that body was added to the geologic picture (Lajoie and West, 1976). Thus the resultant magnetic field contains information about the *total currents* which are a superposition of the *induced* circulating currents and *gathered* currents (Fig. 16c). Present electromagnetic methods recognize interactions, not mere superpositions of currents initially induced in each of the six distinct elements of the *section* depicted in Figure 15.

#### *Separating the elements in the geoelectric section*

Although not an objective in the past, the current main objective of the EM method is to have an ability to detect and evaluate each element of the geoelectric section so that the resistivity environment surrounding the assumed ore may be assessed. In this fashion, for example, we may hope to recognize massive sulfide ore from disseminated non-economic mineralization in a volcanogenic environment.

The EM exploration problem then may be described as a search for procedures to separate the geological signal due to a massive or concentrated sulfide deposit from the geological noise arising from the other elements of the geoelectric section (Fig. 15). The procedures must be sought with the realization that each noise source may shift the phase, alter the amplitude, and change the spatial spectrum of each component of the secondary fields scattered by the concentrated or massive sulfide deposit. If we are to solve this problem completely, we will need to (a) obtain precise data over several



decades of frequency, (b) avoid spatial aliasing of data (i.e. define all lateral variations of signal or noise by dense station spacing), (c) consider employing several configurations of the transmitter and receiver, and (d) use 3D complex models to simulate the real earth. Compromises between complete solutions and economical or practical solutions are to be expected within this framework.

Ward (1979) reviewed recent papers that address the problems encountered by the EM method when faced with a real earth in which all elements of the geoelectric section of Figure 15, are included. His summarized conclusions are shown in Table 1.

*Depth of exploration*

When a plane electromagnetic wave travels through earth materials, the amplitudes of its electric and magnetic vectors are attenuated exponentially as

$$\begin{Bmatrix} \vec{E} \\ \vec{H} \end{Bmatrix} \propto e^{-\beta d}$$

where  $d$  is distance travelled and  $\beta$  is the attenuation coefficient given by

$$\beta = \sqrt{\frac{\sigma\mu\omega}{2}}$$

in which  $\sigma$  is electrical conductivity in mhos/m,  $\gamma$  is magnetic permeability in henry/m,  $\omega = 2\pi f$  is angular frequency, while  $f$  is frequency in Hz.

At a depth  $d = 1/\beta$ , the intensity of the incident electric or magnetic field has fallen off to  $1/e$  of its value at the surface of the earth; this depth is called the skin depth or *depth of penetration* and is denoted by  $\delta$  where

$$\delta = \sqrt{\frac{2}{\sigma\mu\omega}}$$

Assuming the magnetic permeability is that of free space in m.k.s., rationalized units, i.e.  $\mu = \mu_0 = 1.26 \times 10^{-6}$  henry/m, then the skin depth is closely approximated by

$$\delta = 500 \sqrt{\rho/f} ,$$

indicating that lower frequencies are required for greater depth of exploration. At very large distances from a source of electromagnetic waves, attenuation of this type would control the *depth of exploration*. Depth of exploration is defined as the maximum depth a body can be buried and still produce a signal recognizable above the noise. The depth of exploration for a sphere is much less than that for an infinitely extended buried horizontal interface; both the noise level and the response of the body influence the depth of exploration. The matter is even more complicated because the *geometrical decay* of magnetic field amplitude is  $1/R^3$  for a loop source and  $1/R$  for a line source, where R is the distance from the source to a point of interest in the earth. To visualize the relative importance of attenuation and geometrical decay, we have computed each at a depth of 100 m beneath a loop and a line source on the surface of the earth for three frequencies and earth resistivities (Table 2). As one can see, attenuation is insignificant relative to geometrical decay. This fact is not often recognized in EM prospecting. Pridmore et al. (1979) have described it in more detail for a horizontal loop source.

Given that depth of exploration is such a difficult number to define, it is not surprising that only general rules of thumb have arisen in practice. For example, typical depth of exploration statements are: "a conductive

interface can be detected at about 0.3 to 0.5 of the separation between transmitter and receiver," or "the depth of exploration of the EM method is 100 m to 200 m". This is unfortunate for the geologist who must utilize the method. In most instances, the depth of exploration can be determined by numerical modeling if knowledge of it is vital.

#### *Time and frequency domains*

Figure 17 shows how FEM (frequency domain EM) and TEM (time domain EM) systems discriminate between good conductors and poor conductors. We assume that the conductor is a sphere with radius  $R$  and conductivity  $\sigma$ . the TEM response can be approximated by a single exponential decay:

$$h(t) = e^{-t/\tau}$$

where the time constant,  $\tau$  is given by

$$\tau = \frac{\sigma \mu_0 R^2}{\pi}$$

in which  $\mu_0 = 1.26 \times 10^{-6}$  henry/m is the magnetic permeability of free space. The equivalent FEM response is:

$$H(f) = \frac{\left(\frac{1}{\tau}\right)^2}{\left(\frac{1}{\tau}\right)^2 + 4\pi^2 f^2} + j \frac{2\pi \frac{f}{\tau}}{\left(\frac{1}{\tau}\right)^2 + 4\pi^2 f^2}$$

Larger time constants, then, correspond to larger  $(\sigma R^2)$  products.

In Figure 17, we compare FEM and TEM responses of a good conductor ( $\tau = 3.2$  msec) and a poor conductor ( $\tau = 0.64$  msec). For spheres of radii 50 m and 100 m, respectively, these time constants correspond to conductivities of 10 and 0.5 /m, respectively. In the time domain, the poor conductor is characterized by a more rapid decay, while in the frequency domain the peak

quadrature response and maximum slope of the in-phase response occur at a higher frequency for the poor conductor.

There are certain theoretical advantages to TEM, in addition to increased surveying efficiency. For example, noise due to topography, location errors, and coil orientation errors can seriously contaminate in-phase FEM measurements with certain coil configurations but are minimal with TEM because measurements are made with the transmitter current turned off. Furthermore, TEM measurements at late times can eliminate geological noise more effectively than can FEM measurements at low frequencies (Kaufman, 1978).

FEM systems provide better rejection of natural EM field noise, but that advantage is negated by the TEM capability for much greater transmitter current with the same size generator if low duty cycles are used. For example, the Newmont *EMP* TEM system drives 100 amperes through the transmitter loop with only a 2 kw generator because the duty cycle is low.

Hence, even though FEM measurements are related to and derivable from TEM measurements through Fourier transformation, it would appear that there are both practical and theoretical advantages to TEM systems. However, at present, TEM systems are limited to about two decades of spectrum whereas FEM systems can accommodate four decades of spectrum; a field example will be presented later that will illustrate the advantage to be gained by use of a broader spectrum.

#### *Field configurations, natural field methods*

*Introduction:* These methods utilize the earth's natural electric and magnetic fields to infer the electrical resistivity of the subsurface. Figure 18 is a generalized spectrum of natural magnetic field amplitude adapted from Campbell (1967). There is, of course, a corresponding similar electric field

spectrum.

In general, the fields above 1 Hz are due to a) worldwide thunderstorms, b) radio stations, and c) power distribution systems. Below 1 Hz the fields, called micropulsations, are mainly due to the complex interaction of charged particles from the sun with the earth's magnetic field and ionosphere. As Figure 18 shows, the amplitude of the electromagnetic field increases with decreasing frequency below 1 Hz.

These natural fields represent noise for controlled-source electromagnetic (CSEM) methods, but they are the source fields for natural field electromagnetic (NFEM) methods. Because low frequencies are needed for deep penetration, it is easy to see from Figure 18 why NFEM has been used so extensively for crustal studies and deep exploration: the source fields increase at low frequencies for NFEM, while the noise increases at low frequencies for CSEM.

While frequencies below 1 Hz can be useful in regional studies, higher frequencies usually are employed in mineral exploration due to the relatively small target size and because of their greater surveying efficiency and greater resolution.

*The magnetotelluric method:* In the magnetotelluric (MT) method one measures the ratio between orthogonal electric field ( $E_x$ ) and magnetic field ( $H_y$ ) components at the earth's surface over the frequency range  $10^{-3}$  Hz to 10 Hz. The MT apparent resistivity is given by

$$\rho = \frac{0.2 E_x^2}{f H_y^2}$$

where  $f$  is the frequency, and  $E_x$  and  $H_y$  are measured in units of mv/km and gammas, respectively.

*Audiomagnetotellurics* (AMT), the variant of MT most often used in mineral exploration (Strangway, et al., 1973), simply refers to MT in the audio frequency range of 10 Hz to  $10^4$  Hz. The magnetic field is measured with a small coil, while the electric field usually is measured with a 30 m grounded wire. Unfortunately, weak source fields and a lack of sophisticated instruments and interpretation techniques have hindered the application of AMT.

Tensor measurements, i.e. simultaneous measurement of  $E_x$ ,  $E_y$ ,  $H_x$ ,  $H_y$  and  $H_z$ , are necessary to compensate for varying source fields, but they must be coupled with 2D and 3D numerical solutions for interpretation. Through recent advances in electronics, portable tensor AMT receivers will soon be available so that AMT will assume a more prominent role in mineral exploration. It is a simple technique, can be made highly portable, does not require accurate distance measurements, and does not require a transmitter. AMT is particularly useful in searching for flat lying conductors beneath overburden of high resistivity.

*AFMAG*: The *AFMAG* method (Ward et al., 1958) utilizes frequencies near the peak of the natural magnetic field spectrum at about 100 Hz in Figure 18. The tilt angle of the major axis of the ellipse of magnetic field polarization relative to the horizontal is measured by use of orthogonal receiving coils. The tilt angle will vary systematically across subsurface inhomogeneities such that the axes of current flow in the inhomogeneity can be detected and delineated. Because of the distant sources and uniform inducing field, current gathering usually dominates over local induction with the method. However, it can be useful for cheaply and quickly mapping faults and shears and for detecting deep large conductors such as graphitic zones beneath the Athabasca sandstone. An airborne version of *AFMAG* was flown for several

years. The limitations of *AFMAG* have been described by Ward et al. (1966); they include time variant intensities and directions of inducing fields with concomitant changes in locations and intensities of anomalies.

*VLF*: Because very low frequency (VLF) fields in the range 10 to 30 kHz are generated by distant transmitters for navigation and communication, we classify VLF as a natural field method. At least one station can be monitored anywhere on the earth, so the explorationist requires only a receiver to conduct a survey. However, the frequencies are too high for much penetration, so that the method is useful only for shallow geologic mapping, i.e. locating faults and contacts, and for probing for conductors beneath less than 50 meters of highly resistive surface rocks.

A secondary vertical magnetic field is created near a conductor; hence, in the most common VLF technique measurements are made of the tilt angle and ellipticity of the total alternating magnetic field. In practice, one determines the polarization ellipse in a vertical plane oriented in the direction of maximum horizontal magnetic field. Strong conductors tend to rotate the horizontal magnetic field to be perpendicular to their strike. If possible, one should choose a transmitter whose azimuth is roughly in the direction of regional strike. Several airborne VLF systems are available, and are used primarily for geological mapping. Recent 2D numerical modeling studies (Kaikkonen, 1979) have resulted in improved interpretation aids for VLF surveys. However, in many cases VLF anomalies are due to current channeling and hence require 3D models for simulation.

*Field configurations, controlled source, ground methods*

*Introduction*: The number of configurations of transmitter and receiver used in EM prospecting is large (Grant and West, 1965; Ward, 1979; Telford et al., 1976). This leads to confusion concerning the selection of a particular

configuration for a specific exploration problem. However, some semblance of order can be achieved by assigning each particular configuration to one of the four basic configurations illustrated in Figure 19. A few of the possible systems are described, briefly, so that case history data presented later can be appreciated.

For the *fixed vertical loop* method, the axis of the fixed transmitting coil is oriented normal to strike and the receiving coil is moved incrementally along the axis of the transmitting coil. The tilt of the major axis and the ellipticity of the ellipse of magnetic field polarization are measured. Then the transmitting coil is moved to an adjacent line and the measuring process repeated. This is not a standard technique but has been used with success where tried (Pridmore et al., 1979).

With the frequency domain *TURAM* method (Bosschart, 1964) a large rectangular transmitting coil, hundreds or even thousands of meters to a side, is laid out on the ground and the field strength ratio and phase difference are recorded between a pair of receiving coils 30 m to 100 m apart, along traverses normal to one of the long sides of the rectangular loop.

The frequency domain Kennecott *Vector EM* system (Hohmann et al., 1978) uses a large fixed rectangular loop of Turam dimensions for reconnaissance exploration. The system can also be used with a rotating vertical loop. The single receiving coil permits measurement of absolute amplitude and phase of the vertical component of magnetic field at four frequencies. These absolute quantities are then converted to field strength ratios and phase differences as in *TURAM*.

The time domain Newmont *EMP* system uses a large fixed rectangular transmitting loop, hundreds of meters to a side. The received signals are the three orthogonal components of magnetic field recorded at 32 discrete time



channels after termination of each transmitted current pulse (Nabighian, 1977).

With the time domain Russian *MPP01* (Velikin and Bulgakov, 1967) and the Australian *SIROTEM* (McCracken and Buselli, 1978), a single rectangular loop 50 m to 200 m to a side, is used first as a transmitter and then at appropriate time delays, as a receiver. Sirotem also offers the opportunity to use separate transmitting and receiving loops separated by 100 m to 200 m.

The controlled source audiomagnetotelluric (CSAMT) technique (Golstein and Strangway, 1975) circumvents some of the problems with natural field AMT. It is most useful in exploring for flat-lying conductors.

*Field configurations, controlled source, airborne:* Recent papers dealing with AEM (Airborne Electromagnetic) systems have included those by Ward (1969), Paterson (1971), Ghosh (1972), and Becker (1980). We shall identify herein only three basic types of systems and reference some of the present models belonging to these types.

*Rigid boom systems:* The transmitting and receiving coils are attached to a rigid boom to minimize translation and rotation of one coil relative to the other. In the most common type of rigid boom system, the coils are separated by about 10 m and are attached to a large boom or bird which is towed beneath a helicopter as in Figure 20a. The *DIGHEM* system is of this type. Secondary magnetic fields both in-phase and quadrature with respect to the primary field are recorded at one or more frequencies of the order of 1000 Hz to 5000 Hz. The helicopter flies at a nominal height of 70 m while the bird flies at a nominal height of about 35 m. Signals less than 1 part per million of the primary field can be recorded.

In another type of rigid boom system, the coils are mounted on structures attached to the airframe of the helicopter or fixed wing aircraft as in Figure

20b. A third type of rigid boom system utilizes two coplanar coils mounted on the wing tips of a fixed wing aircraft as in Figure 20c. *TURAIR* (Figure 20e) is akin to the ground *TURAM* method (Bosschart and Seigel, 1971). Two receiving coils, mounted on opposite ends of a 10 m bird towed beneath a helicopter, allow airborne measurement of field strength ratio and phase difference along traverse lines normal to the long sides of a large rectangular loop.

Figure 20d illustrates a small bird, carrying the receiving coil, towed behind and beneath an aircraft. These systems measure quadrature secondary magnetic field, only, when operating in the frequency domain. The *INPUT* system is a TEM version of this *towed bird* type of system. Separation between coils is nominally 150 m with aircraft heights of 125 m to 150 m.

#### *Geological noise in electromagnetic surveys*

The detectability of an exploration target in a particular environment is determined by the ratio of signal to noise, which in turn depends upon two factors: (1) the characteristics of the target response, and (2) the characteristics of the noise. In order to increase the probability of discovery, we must increase the signal and reduce the noise in a cost-effective manner. In geophysical exploration with the EM method, we find disturbance field noise, instrumental noise, cultural noise, topographical noise, and geological noise. For the purposes of this paper, only geological noise requires discussion. By geological noise we mean the EM response of any conductive feature in the earth other than the economic target. Graphite and permeable shear zones are important sources of geological noise, while noise arising from lateral variations in an overburden of low resistivity often is the most important type of noise in conductive terrain, such as much of Australia.

Overburden of low resistivity tends to attenuate responses from bedrock, but its most deleterious effect is to produce EM anomalies due to lateral porosity changes, thickness variations, and differential weathering. Sources of geological noise in the overburden generally are not as conductive as massive sulfides, but they are shallow and thus may produce anomalies comparable to or greater than anomalies due to good conductors in bedrock.

Some means must be used to discriminate among the numerous EM anomalies that arise in surveys where overburden is thick and conductive. The common means of discrimination are: (1) correlating with other types of information, (2) selecting only good conductors, and (3) selecting conductors having the correct geometry. In the first method, EM anomalies that have associated magnetic, gravity, geochemical, or induced polarization anomalies, for example, are selected for further investigation. Discrimination by conductivity and geometry is an important research and development topic. As indicated above, conductivity discrimination is by decay rate in the time domain and by amplitude-phase relations with frequency in the frequency domain.

*Vector EM* data, at four frequencies, from a deeply weathered nickel prospect in Western Australia (Hohmann et al., 1978) are shown in Figure 21. An aeromagnetic survey and trenching defined a prospective ultramafic body between 2W and 9.5W. Resistivities are as low as 5  $\Omega$ -m and are highly variable due to differential weathering. The water table is about 15 m deep. The basal contact of the ultramafic was drilled and intersected on this line at 9.5 W and at several other locations along strike without encountering mineralization. Geological noise is very high in the electromagnetic data due to the deep differential weathering. However, geological noise is much less at the lower frequencies, so that it would be possible to detect a conductor

with a good response at low frequencies, provided it were not too deep.

Figure 21 illustrates an unfortunate problem for nickel exploration in Western Australia. Magmatic segregation deposits occur at the basal contact of an ultramafic body but often there is, as at 9.5W in this case, a strong anomaly due to a shallow conductor, probably a permeable shear zone along the entire contact. Detection of a small nickel deposit beneath this shallow conductor would be quite difficult with the EM method.

In contrast, Figure 22 (Hohmann et al., 1978) shows four-frequency *Vector EM* data over the Freddie Well deposit, a shallow massive sulfide body in Western Australia, at a location where overburden conditions are more favorable for application of the EM method. Massive and disseminated mineralization occurs over a 30 m interval centered at 0 on the line. Its electrical conductivity is high due to well-connected pyrite and pyrrhotite lenses. Background resistivity ranges between 30  $\Omega$ -m on the west end of the line and 300  $\Omega$ -m to the east. The large responses at 26 Hz and 77 Hz show that the anomaly is due to a very good conductor of the type that could be detected even through the geological noise of Figure 21. Numerical modeling suggests that the bulk resistivity of the body is 0.1 to 0.3  $\Omega$ -m, and its depth is about 30 m.

The geometrical aspects of EM anomalies also can be used to discriminate between geological noise and target response. For example, the 100 m by 100 m loop, with which the *SIROTEM* data of Figure 23 were taken, averages the magnetic field over a large area. Hence the narrow response of a surficial conductor is suppressed with respect to the broad response of a deep conductor. Unfortunately, conductive overburden produces broad anomalies in some instances.

The Newmont *EMP* system (Nabighian, 1977) measures the magnetic fields in three orthogonal directions to obtain geometrical information about conductors, which aids conductor discrimination. Further, Nabighian (1978) finds that at late times a layered-earth response can be subtracted from the total response; analysis of the residual anomaly yields the correct parameters for the conductor if current channeling is not significant. Figure 24 shows *EMP* anomalies in the three orthogonal components at 5.63 msec over the Mutooroo deposit near Broken Hill in New South Wales, Australia. The overburden response has disappeared by 5.63 msec. The location of the bedrock conductor lies directly beneath the peak of the Y component and beneath the crossover in the Z component. Figure 25 shows that this location lies downdip of the outcrop, as it should since the weathered sulfides are not highly conductive. The strike of the conductor is clearly evident in the EM data as Figure 25 shows. Kuo and Cho (1980) discuss the quantitative interpretation of the EM data over this deposit.

Several other state-of-the-art means of enhancing the ratio of signal to noise are given in the section on applications below.

A geological noise source which becomes of importance in rigid boom AEM systems arises in magnetic bodies. Figure 26, from Fraser (1979), shows a large magnetic signature and its suppression by the *DIGHEM II* system. Figure 26 records (1) total magnetic intensity, (2) bird terrain clearance, (3) coaxial coil in-phase, (4) coaxial coil quadrature, (5) horizontal coplanar coil in-phase, (6) horizontal coplanar coil quadrature, (7) the difference between channel (3) and one half of channel (5), (i.e., in-phase difference), (8) the difference between channel (4) and one half of channel (6) (i.e., quadrature difference), and (9) the apparent resistivity deduced from the horizontal coplanar coil pair. Unless more than one coil configuration is

used, this noise source cannot be suppressed and can result in obscuring anomalies due to conductive targets as Fraser notes.

#### APPLICATIONS

In this section we present a limited number of examples of solutions to difficult exploration problems, by use of advanced EM systems.

*Airborne electromagnetics in areas of conductive overburden:* Early application of the EM method in the Precambrian Shield of Canada and Scandinavia met with remarkable success because the target areas were characteristically devoid of conductive overburden. As Shield exploration gradually shifted to areas covered by deep conductive overburden, success at first diminished. Then as experience was acquired with much improved and more versatile equipment, success again became remarkable but at increased cost. Fraser (1979) provides an example of application of the frequency domain *DIGHEM II* airborne system in an area of conductive overburden. The example is the AEM flight records over the Montcalm deposit in Ontario, Canada (Fig. 27). The channel identification is the same as in Figure 26. Insofar as both coil pairs respond to a layered earth in the same manner except that the response of the horizontal coplanar coil pair is twice that of the coaxial coil pair, the difference channels largely eliminate the effect of the overburden which dominates the quadrature channels (4) and (6) and degrades the ratio of signal to noise of the in-phase channels (3) and (5). The resistivity channel is very helpful in mapping overburden type in such areas. Smee and Sinha (1979) discuss the clay overburden problem in light of recent technology.

*Ground electromagnetics in deeply weathered areas:* Figure 23 contains data from a *SIROTEM* survey over the Elura deposit in New South Wales, Australia (McCracken and Buselli, 1978). This massive sulfide deposit is

highly conductive ( $0.1 \Omega\text{-m}$ ) but lies beneath a 100 m weathered layer and hence presents an extremely difficult target. At the 2.0 msec and 3.4 msec sampling time the response is in the hundreds of microvolts of received signal per ampere of transmitted current and is due mostly to the conductive weathered rock; the response of the deposit tends to be obscured. At the 7.0 msec sampling time, the response of the weathered layer is mostly gone while the response of the deposit is decreasing; the ratio of the 7.0 msec response to the 19.0 msec response can provide an estimate of the conductivity of the deposit. Unless a precise broadband instrument had been used, the separation of weathered layer response from sulfide deposit response would not have been possible.

*Detecting ore adjacent to disseminated sulfides in conductive terrain:*

Resolution of adjacent conductors in some exploration problems is essential if one is to minimize drilling of uneconomic sulfides and maximize the probability of intersecting ore. One such problem arose in the Foothills Copper Belt of California (Pridmore, et al., 1979). The deposit in question is a typical volcanogenic massive sulfide pod which grades laterally into a variably disseminated sulfide zone. The problem is to resolve the massive from the disseminated sulfides.

Figure 28 contains contours of tilt angle as a function of frequency distance for the fixed vertical coil configuration described earlier. The massive sulfide response occurs at BB' over the frequency range 30 Hz to 1000 Hz and is of small amplitude. The disseminated sulfide response occurs at CC', is ten times larger in amplitude, and occurs at frequencies above 2000 Hz. The overburden and weathered bedrock response occurs at AA' and spans frequencies from  $10^3$  Hz to  $10^5$  Hz. By exciting the earth over nearly four decades of frequency and making very precise measurements of tilt angle

(precise to  $0.1^\circ$ ), it is possible to separate the effects of massive from disseminated sulfides and to recognize the overburden and bedrock response in the data. *TURAM* and induced polarization methods were unsuccessful in this difficult problem of resolution.

*Airborne detection of conductors beneath deep resistive occur:* Uranium occurs in association with graphitic pelites in the lower Aphebian rocks beneath the Athabasca sandstones of the Athabasca basin of Saskatchewan, Canada. From outcrops around the basin, the Aphebian metamorphic rocks become increasingly buried until toward the center of the basin they may be covered by more than 1000 m of sandstone. Fortunately the sandstone is resistive ( $3000 \Omega\text{-m}$ ) so that one can "see through" it with AEM methods rather readily, except in those parts of the basin where the overburden is deep and conductive. *INPUT* anomalies, due to the graphitic pelites, reportedly have been found beneath 200 m of Athabasca sandstone cover. Figure 29 portrays an example of the ability of *INPUT* to see through resistive cover of about 125 m in thickness.

*Uses of airborne electromagnetic systems:* Initially, AEM systems were used solely to search for anomalies over massive sulfide deposits; this is still their most common use. We refer to this as AEM profiling. In later years, the *INPUT*, *DIGHEM II* and *TRIDEM* systems have been used additionally to produce maps of resistivity from the air. Seigel and Pitcher (1978) report on the use of *TRIDEM* to map sand, clay, bedrock, and lignite. Fraser (1978, 1979) reports on the use of *DIGHEM II* to estimate surficial resistivity and thereby remove surficial conductors from consideration when one is engaged in sulfide search. He also reports on the use of *DIGHEM II* in mapping permafrost, sand, and gravel. Palacky and Kadkaru (1979) report on the use of *INPUT* in estimating overburden and bedrock resistivities.



## REFERENCES

- Becker, A., 1980, Airborne electromagnetic methods, *in* P. J. Hood (ed.) Geophysics and Geo-chemistry in the Search for Metallic Ores: Geol. Surv. Can., Econ. Geol. Rpt. 31, p. 33-43.
- Bosschart, R. A., 1964, analytical interpretation of fixed source electromagnetic prospecting data, Ph.D. thesis, Delft, Uitgeverij Waltman, 103 p.
- Bosschart, R. A. and Seigel, H. O., 1971, Turair; a semi-airborne electromagnetic method for deep mineral exploration: Scintrex Ltd. brochure.
- Campbell, W. H., 1967, Geomagnetic pulsations: *in* Physics of Geomagnetic Phenomena, Matsushita and Campbell, eds., p. 822-909.
- Coggan, J. H., 1973, A comparison of IP electrode arrays: Geophysics, v. 38, p. 737-761.
- Edwards, R. N., and Howell, E. C., 1976, A field test of the magnetometric resistivity (MMR) method: Geophysics, v. 41, p. 1170-1183.
- Fox, R. C., Hohmann, G. W., Killpack, T. J., and Rijo, L., 1980, Topographic effects in resistivity and induced polarization surveys: Geophysics, v. 45, p. 75-93.
- Fraser, D. C., 1978, Resistivity mapping with an airborne multicoil electromagnetic system: Geophysics, v. 43, p. 144-172.
- Fraser, D. C., 1979, The multicoil II airborne electromagnetic system, Geophysics, v. 44, p. 1367-1394.
- Goldstein, M. A. and Strangeway, D. W., 1975, Audio-frequency magnetotellurics with a grounded electric dipole source: Geophysics, v. 40, p. 669-683.
- Hohmann, G. W., 1975, Three-dimensional induced polarization and electromagnetic modeling: Geophysics, v. 40, p. 309-324.
- Hohmann, G. W., 1977, Numerical IP modeling: Univ. of Ariz., IP Short Course Proceedings.
- Hohmann, G. W., Van Voorhis, G. D., and Nelson, p. H., 1978, A vector EM system and its field applications: Geophysics v. 43, p. 1418-1440.
- Kaikkonen, P., 1979, Numerical VLF modeling: Geophysical Prospecting, v. 27, p. 815-834.
- Kaufman, A., 1978, Frequency and transient responses of electromagnetic fields created by currents in contained conductors: Geophysics, v. 43, p. 1002-1010.
- Kuo, J. T., and Cho, D. H., 1980, Transient time domain electromagnetics: Geophysics, v. 45, p. 271-291.

- Lajoie, J. J. and West, G. F., 1976, The electromagnetic response of a conductive inhomogeneity in a layered earth: *Geophysics*, v. 41, p. 1133-1156.
- McCracken, K. G., and Buselli, G., 1978, Australian exploration geophysics - current performance and future prospects: Second Circum - Pacific Energy and Minerals Resources Conference, July 30-Aug. 4, Honolulu.
- Nabighian, M. N., 1977, The Newmont EMP method *in* Geophysics applied to detection and delineation of non-energy, non-renewable resources: Report on Grant AER76-80802 from the Nat'l Science Foundation; Dept. Geol. and Geophys., Univ. of Utah.
- Nabighian, M. N., 1978, Newmont EMP-Modeling, in Lecture notes from the U.S.-Australia electromagnetics workshop, eds. B. Braham, R. Haren, D. Lappi, H. Lemaire, D. Payne, A. Raiche, B. Spies, and K. Vozoff: *Bull. Aust. Soc. Explor. Geophys.* v. 9, p. 1-33.
- Nelson, P. H., 1977, Induced polarization effects from grounded structures: *Geophysics*, v. 42, p. 1241-1253.
- Palacky, G. J., and Kadekar, K., 1979, Effect of tropical weathering on electrical and electromagnetic methods: *Geophysics*, v. 44, p. 69-88.
- Paterson, N. R., 1971, Airborne electromagnetic methods as applied to the for sulphide deposits: *Can. Inst. Min. Met. Trans.*, v. 64, p. 1-10.
- Pelton, W. H., Ward, S. H., Hallof, P. G., Sill, W. R., and Nelson, P. H., 1978, Mineral discrimination and removal of inductive coupling with multifrequency IP: *Geophysics*, v. 43, p. 588-609.
- Pridmore, D. F., Ward, S. H., and Motter, J. W., 1979, Broadband electromagnetic measurements over a massive sulfide prospect,: *Geophysics*, v. 44, p. 1677-1699.
- Seigel, H. O., 1974, The magnetic induced polarization (MIP) method: *Geophysics*, v. 39, p. 321-339.
- Seigel, H. O., and Pitcher, D. H., 1978, Mapping earth conductivities using a multifrequency airborne electromagnetic system: *Geophysics* v. 43, p. 563-575.
- Smee, B. W., and Sinha, A. K., 1979, Geological, geophysical and geochemical considerations for exploration in clay-covered areas: a review: *Can. Inst. Min. Met. Bull.*, v. 72, p. 67-82.
- Strangway, D. W., Swift, C. M., and Holmer, R. C., 1973, The application of audio-frequency magnetotellurics (AMT) to mineral exploration: *Geophysics*, v. 38, p. 1159-1175.
- Sumner, J. S., 1976, Principles of induced polarization for geophysical exploration: New York, Elsevier Scientific Publishing Company, 277 p.

- Telford, W. M., Geldart, L. P., Sherrif, R. e., and Keys, D. A., 1976, Applied geophysics: London, Cambridge Univ. Press, 860 p.
- Van Voorhis, G. D., Nelson, P. H., and Drake, T. L., 1973, Complex resistivity spectrum of porphyry copper mineralization: Geophysics, v. 38, p. 49-50.
- Velikin, A. B., and Bulgakov, Y. I., 1967 Transient method of electrical prospecting (one loop version): International seminar on geophysical methods of prospecting for ore minerals, Moscow, 1967.
- Ward, S. H., Cartier, W. O., Harvey, H. A., McLaughlin, G. H., and Robinson, W. A., 1958, Prospecting by use of natural alternating fields of audio and sub-audio frequencies; Can. Inst. Min. Met. Bull., v. 51, p. 487-494.
- Ward, S. H., O'Donnell, J., Rivera, R., Ware, G. H., and Fraser, D. C., 1966, AFMAG - Applications and limitations: Geophysics, v. 31, p. 576-605.
- Ward, S. H., 1969, Low-frequency airborne electromagnetic methods: Advances in Geophysics, v. 13, p. 41-88, New York, Academic Press.
- Ward, S. H., 1979, Ground electromagnetic methods and base metals, *in* P. J. Hood (ed.) Geophysics and Geochemistry in the Search for Metallic Ores; Geol. Surv. Can., Econ. Geol. Rpt. 31, p. 45-62.
- Wynn, J. C., and Zonge, K. L., 1975, EM coupling, its intrinsic value, its removal and the cultural coupling problem: Geophysics, v. 40, p. 831-850.

## FIGURE CAPTIONS

- Fig. 1. Sine wave decomposed into in-phase and quadrature components. Amplitude is designated by  $A$ , phase by  $\phi$ , period by  $T$ , and frequency by  $f$ .
- Fig. 2. Typical time domain waveform.
- Fig. 3. Interpretation models:  $\rho$  denotes resistivity and  $\phi$  denotes IP response, 1D - one dimensional, 2D - two dimensional, 3D - three dimensional.
- Fig. 4. Pseudosection contours of the IP response of a large 2D body, of depth extent (DE) equal to 4 with and without overburden. All length units in multiples of a dipole length.  $B_2(\%)$  is the percentage of the intrinsic IP response of the body. (Computed by C. M. Swift, Jr.).
- Fig. 5. EM coupling in mrad of phase due to a 3D conductive ( $1 \Omega\text{-m}$ ) prism in a  $100 \Omega\text{-m}$  earth. Prism width 2000 ft (610 m), depth extent 3000 ft (915 m), length 6000 ft (1820 m), and depth 1000 ft (305 m).
- Fig. 6. Extrapolation method of removing Em coupling from IP data.
- Fig. 7. Typical in-situ IP phase spectra for various types of mineralization. (from Pelton et al., 1978).
- Fig. 8. Apparent resistivity anomaly due to a 2D valley with 30 degree slopes (after Fox et al., 1980).
- Fig. 9. Total electric field IP response  $B_2(\%)$  and quadrature field direction in the earth for a  $1 \times 1 \times 5$  body with no resistivity contrast. Large numbers in pseudosection are IP response for the transmitter dipole considered. Broken arrows show direction of primary field.
- Fig. 10. Effect of depth on IP response. Depths of .5, 1, and 2 dipole lengths for a prism with dimensions:  $W = 2$ ,  $DE = 4$ ,  $L = 5$ ,  $D = 1$ ,  $\rho_2/\rho_1 = 1$ .
- Fig. 11. Peak dipole-dipole IP response versus resistivity contrast for sphere, 3D prism, and two 2D bodies.
- Fig. 12. Superposition of IP responses due to two conductive prisms:  $W = 1$ ,  $DE = 4$ ,  $L = 5$ ,  $D = 1$ ,  $\rho_2/\rho_1 = 0.2$ .
- Fig. 13. IP response from deep sulfide mineralization beneath resistive overburden - Kennecott Safford, Arizona, porphyry copper deposit (courtesy Kennecott Corp.).
- Fig. 14. IP response from sulfide mineralization beneath low-resistivity cover - Lakeshore, Arizona, porphyry copper deposit.

- Fig. 15. The generalized geological model used for the electromagnetic method in the search for massive sulfides.
- Fig. 16. a) Circulating or vortex currents associated with electromagnetic induction in a conductor in a resistivity half-space. The vortex currents add the anomalous  $\Delta E$  to the normal  $E$  recorded by the receiving coil.
- b) Uniform currents induced in a half-space by a transmitting coil. The uniform currents add the anomalous  $\Delta E$  to the normal  $E$  recorded by the receiving coil.
- c) A combination of vortex and uniform currents induced in an inhomogeneous half-space. Both the vortex and the uniform currents, in interaction, contribute to  $\Delta E$ . This is also a pictorial representation of current gathering.
- Fig. 17. Time and frequency domain responses for good and poor conductors.
- Fig. 18. Generalized spectrum of natural magnetic fields (after Campbell, 1967).
- Fig. 19. The four basic field configurations used in electromagnetic exploration consist of: a) coplanar horizontal, coplanar vertical, or coaxial loop pairs, b) a large rectangular source loop to which a single horizontal or vertical receiving coil is referenced, c) a single loop which is used sequentially as transmitter and as receiver in the time domain and d) a grounded wire source to which electric and magnetic field components are referenced.
- Fig. 20. Basic configurations of airborne electromagnetic systems (adapted from Ghosh, 1972).
- Fig. 21. *Vector EM* data obtained in area of high geological noise (after Hohmann, et al., 1978).
- Fig. 22. *Vector EM* survey over the Freddie Well massive sulfide deposit in Western Australia (after Hohmann et al., 1978).
- Fig. 23. Profiles at four time delays of single loop *SIROTEM* survey over the Elura massive sulfide deposit, New South Wales, Australia (after McCracken and Buselli, 1978).
- Fig. 24. Profiles of three orthogonal magnetic field components obtained with the Newmont *EMP* system over the Mutooroo deposit near Broken Hill, S.A., Australia (courtesy Newmont Exploration, Ltd.).
- Fig. 25. Plan view of interpreted position of conductor deduced from Newmont *EMP* results, relative to weathered outcrop positions at the Mutooroo deposit near Broken Hill, S.A., Australia (courtesy Newmont Exploration, Ltd.).
- Fig. 26. Profile record from a *DIGHEM II* flight (after Fraser, 1979).

- Fig. 27. Profile record from a *DIGHEM II* flight perpendicular to Montcalm orebody, Ontario, Canada. The hachures define the contribution from conductive overburden (after Fraser, 1979).
- Fig. 28. Contours of tilt angle as a function of frequency and distance obtained with the University of Utah 14 frequency system across a volcanogenic sulfide deposit in the foothills copper belt of California (after Pridmore et al., 1979).
- Fig. 29. *INPUT* profile across graphitic pelite of the Aphebian metamorphic rocks beneath the Cambrian Athabaska sandstone, Saskatchewan, Canada (courtesy Questor Surveys Limited, Asamera Oil Corporation Limited, Saskatchewan Mining Development Corporation, Kelvin Energy, and E. B. Explorations).

Table 1. Summary of Effects of Extraneous Features in Electromagnetic Search for Massive Sulfides

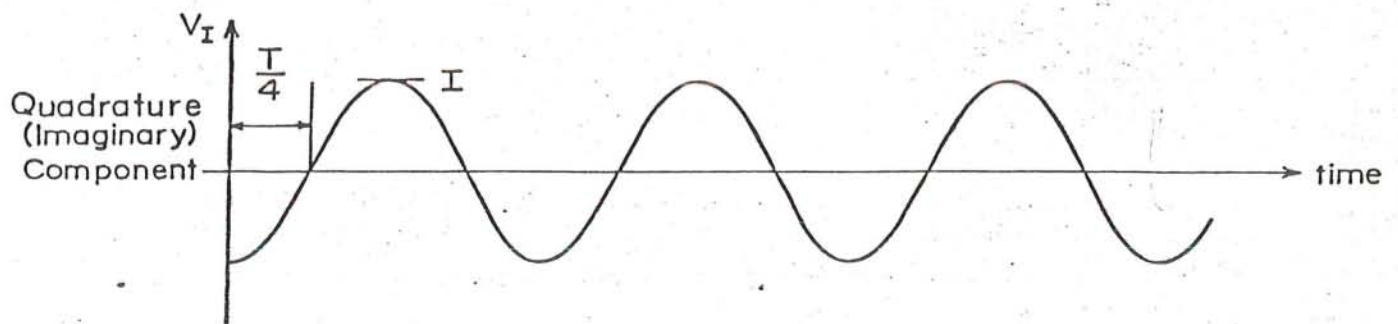
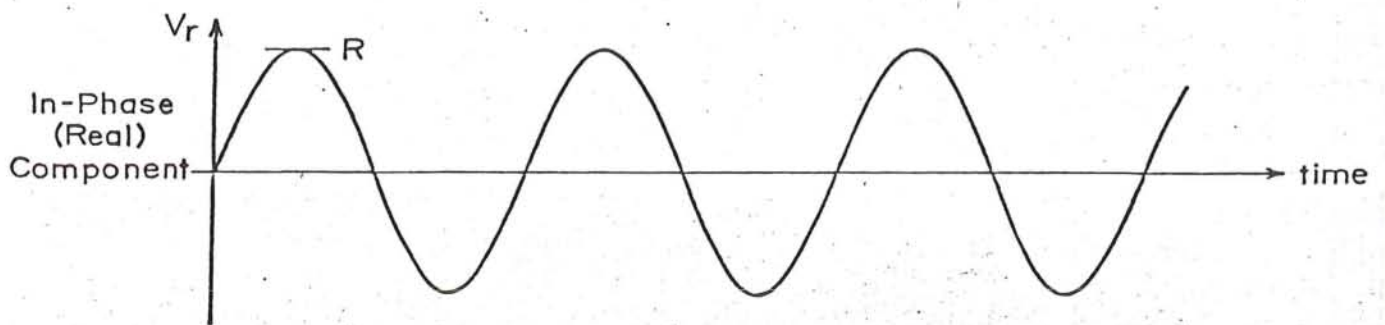
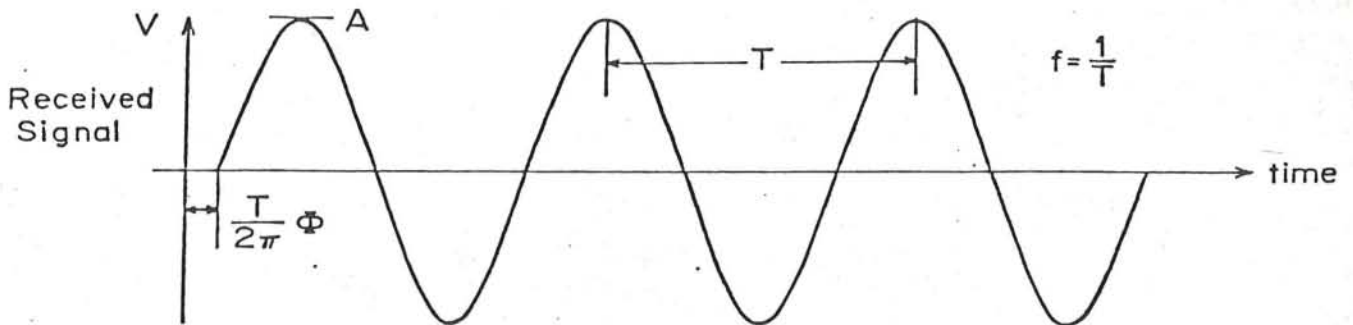
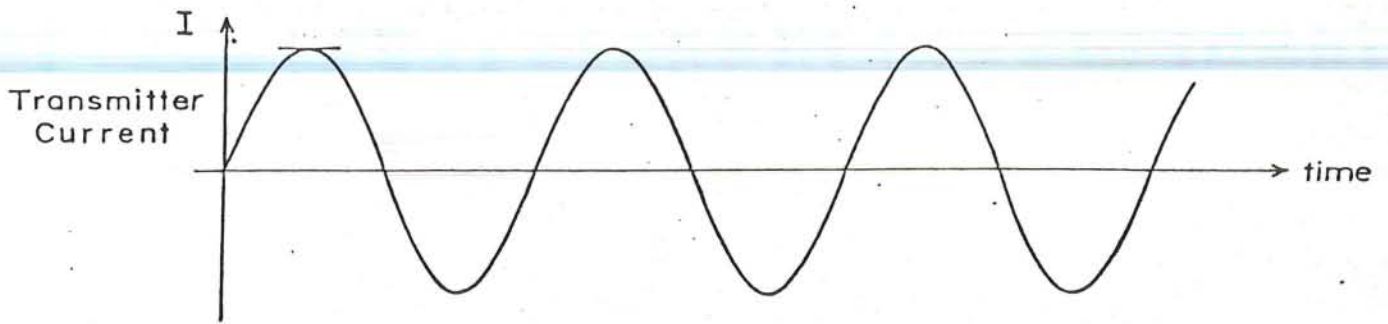
<u>Feature</u>	<u>Effect</u>	<u>Interpretation problem</u> <u>re massive sulfide body</u>
Overburden	rotates phase decreases amplitude	{ depth estimates invalidated conductivity and thickness estimates invalidated
Host rock	rotates phase increases amplitude for shallow conductors increases or decreases amplitude for deep conductors changes shape of profiles fall-off laws changed	{ depth estimates invalidated conductivity and thickness estimates invalidated dip estimates invalidated
Surface and buried topography	introduces geologic noise	{ depth estimates invalidated conductivity and thickness estimates invalidated dip estimates invalidated may obscure sulfide anomalies
Halo	rotates phase increases amplitude	{ depth estimates invalidated conductivity and thickness estimates invalidated dip estimates invalidated
Weathered host rock	introduces geologic noise	{ may obscure sulfide anomalies may invalidate all quantitative interpretation
Faults, shears, graphitic structures	introduces geologic noise	{ may invalidate all quantitative interpretation may obscure sulfide anomalies

**TABLE 2 : Attenuation and Geometrical Decay**

	$\rho = 1000, f=1000$	$\rho = 100, f=10,000$	$\rho = 1000, f=10$
Attenuation	$H_{100}/H_0 = 0.8$	$H_{100}/H_0 = 0.14$	$H_{100}/H_0 = 0.98$
Geometrical Decay Loop source	$H_{100}/H_0 = 10^{-6}$	$H_{100}/H_0 = 10^{-6}$	$H_{100}/H_0 = 10^{-6}$
Geometrical Decay Line source	$H_{100}/H_0 = 10^{-2}$	$H_{100}/H_0 = 10^{-2}$	$H_{100}/H_0 = 10^{-2}$

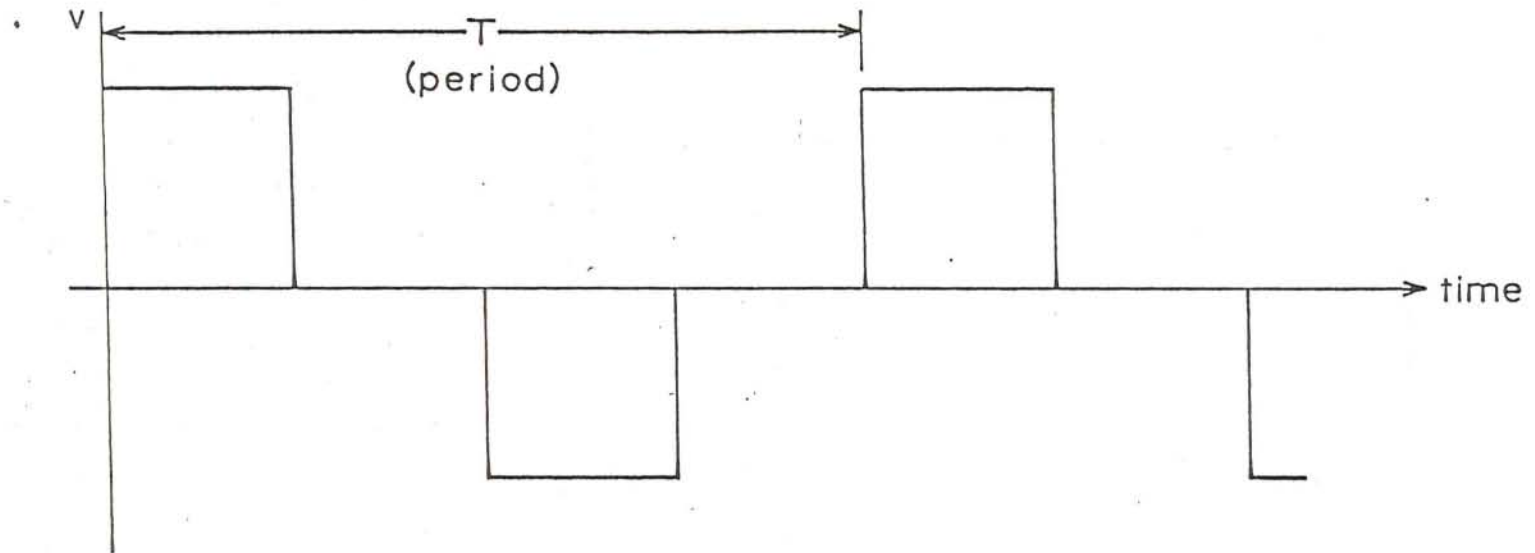


# TRANSMITTER AND RECEIVED WAVEFORMS

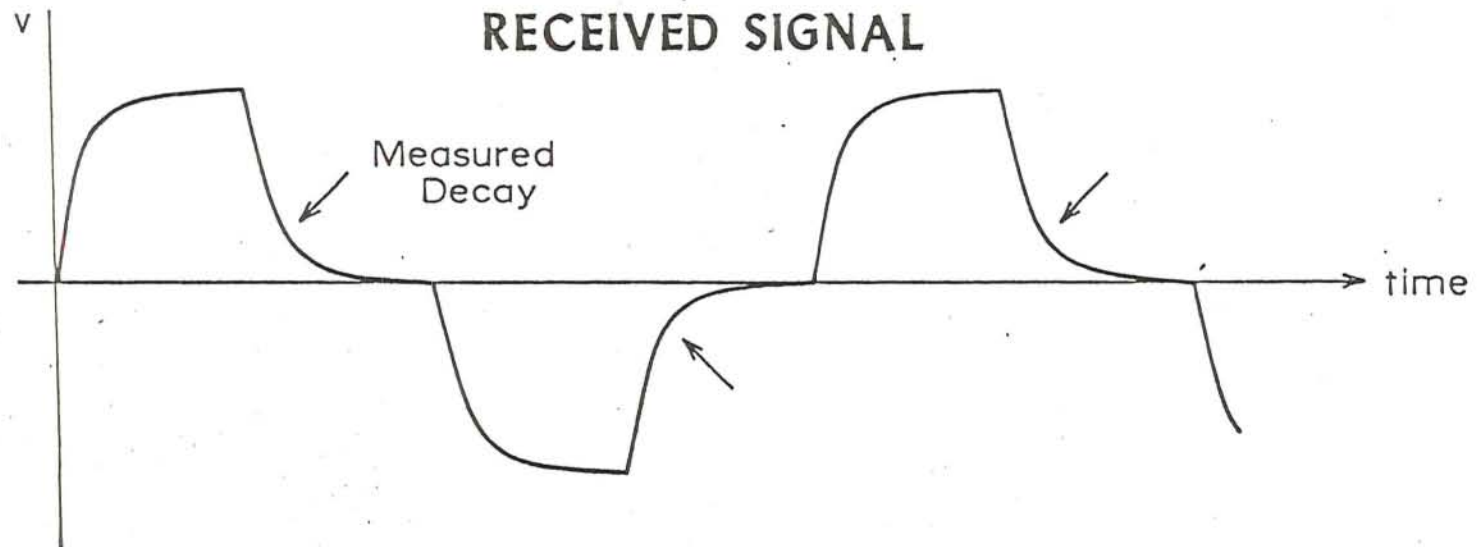


# TRANSMITTER AND RECEIVED WAVEFORMS

## TRANSMITTER CURRENT

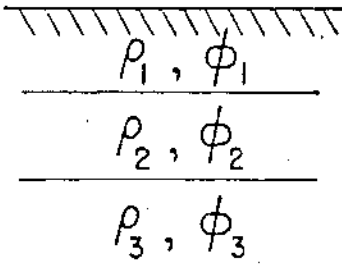


## RECEIVED SIGNAL

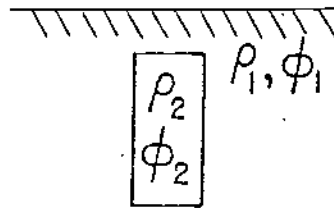


# INTERPRETATION MODELS

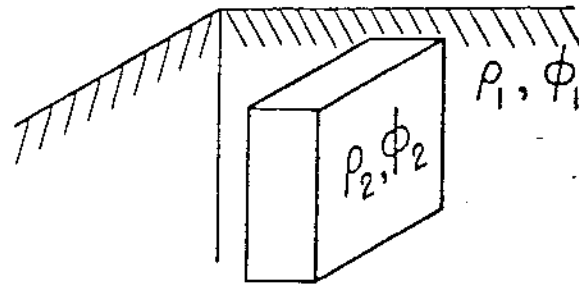
1D



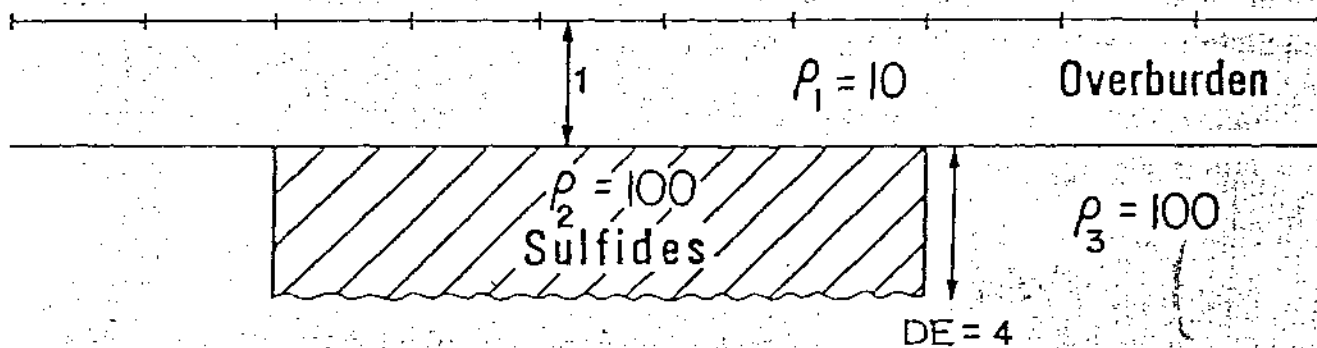
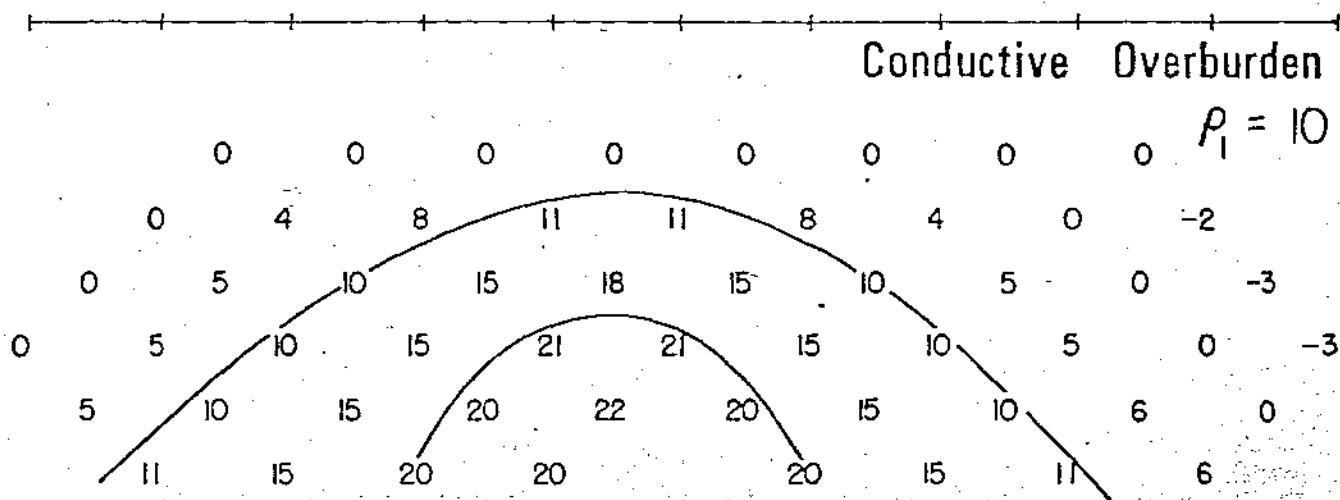
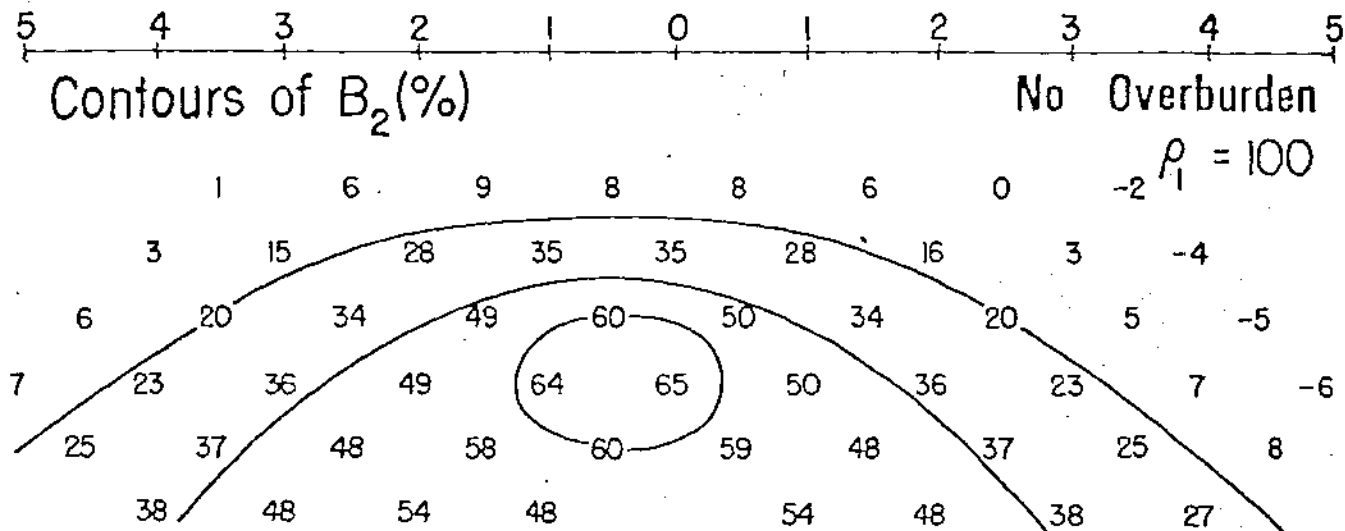
2D



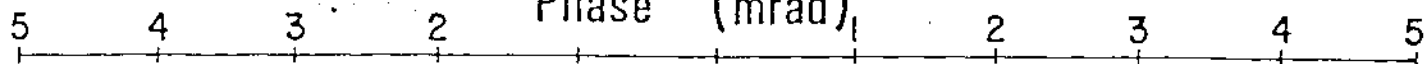
3D



# EFFECT OF OVERBURDEN ON IP

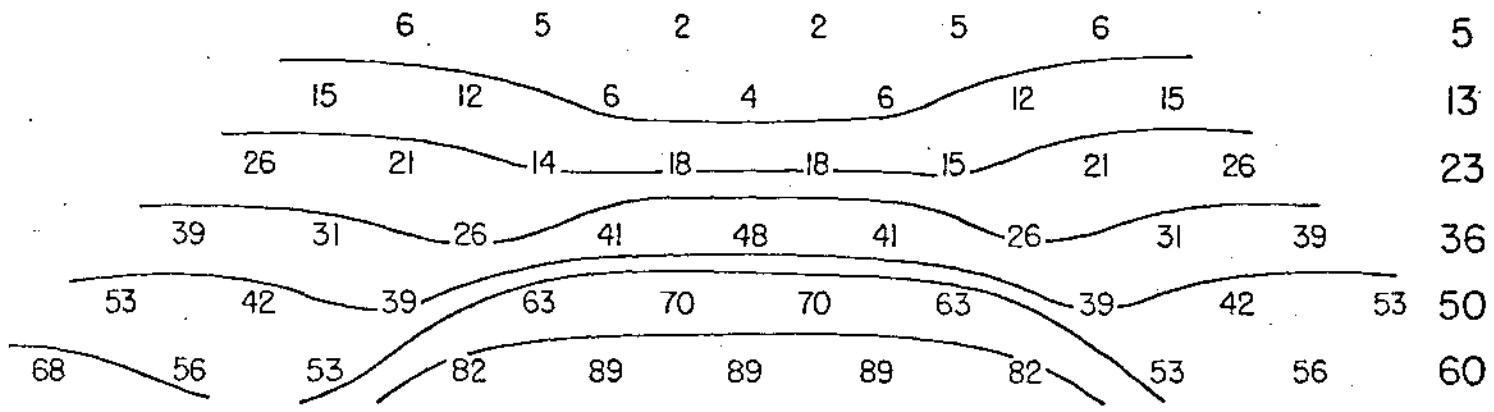


Contours of Phase (mrad)

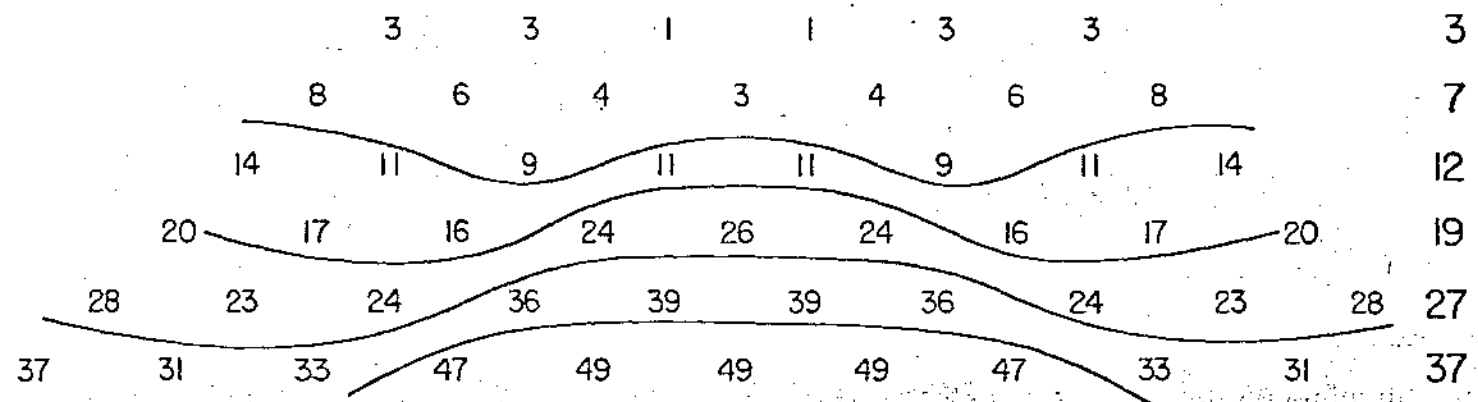


$f = 1.0 \text{ hz}$

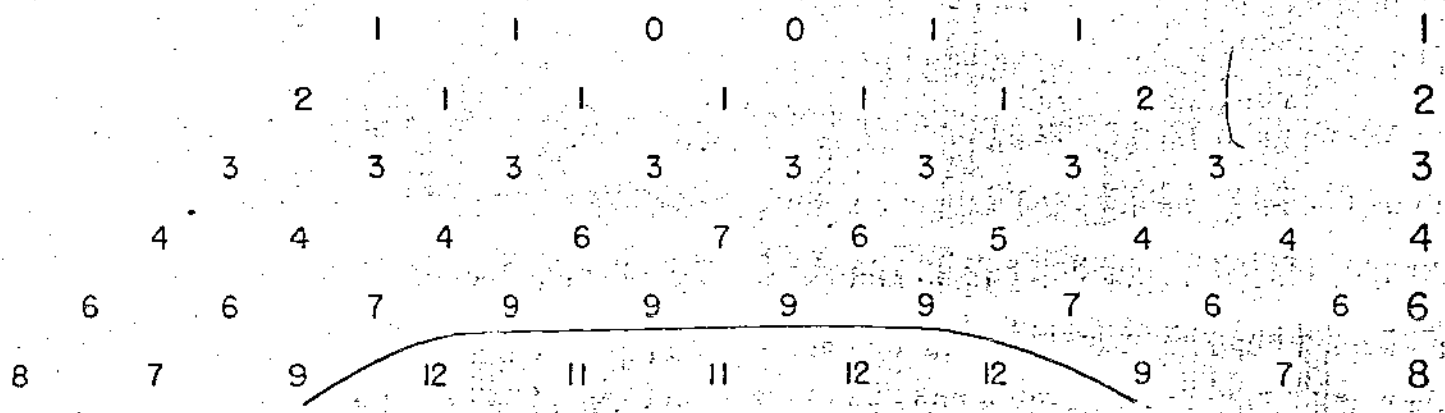
Half-space Value



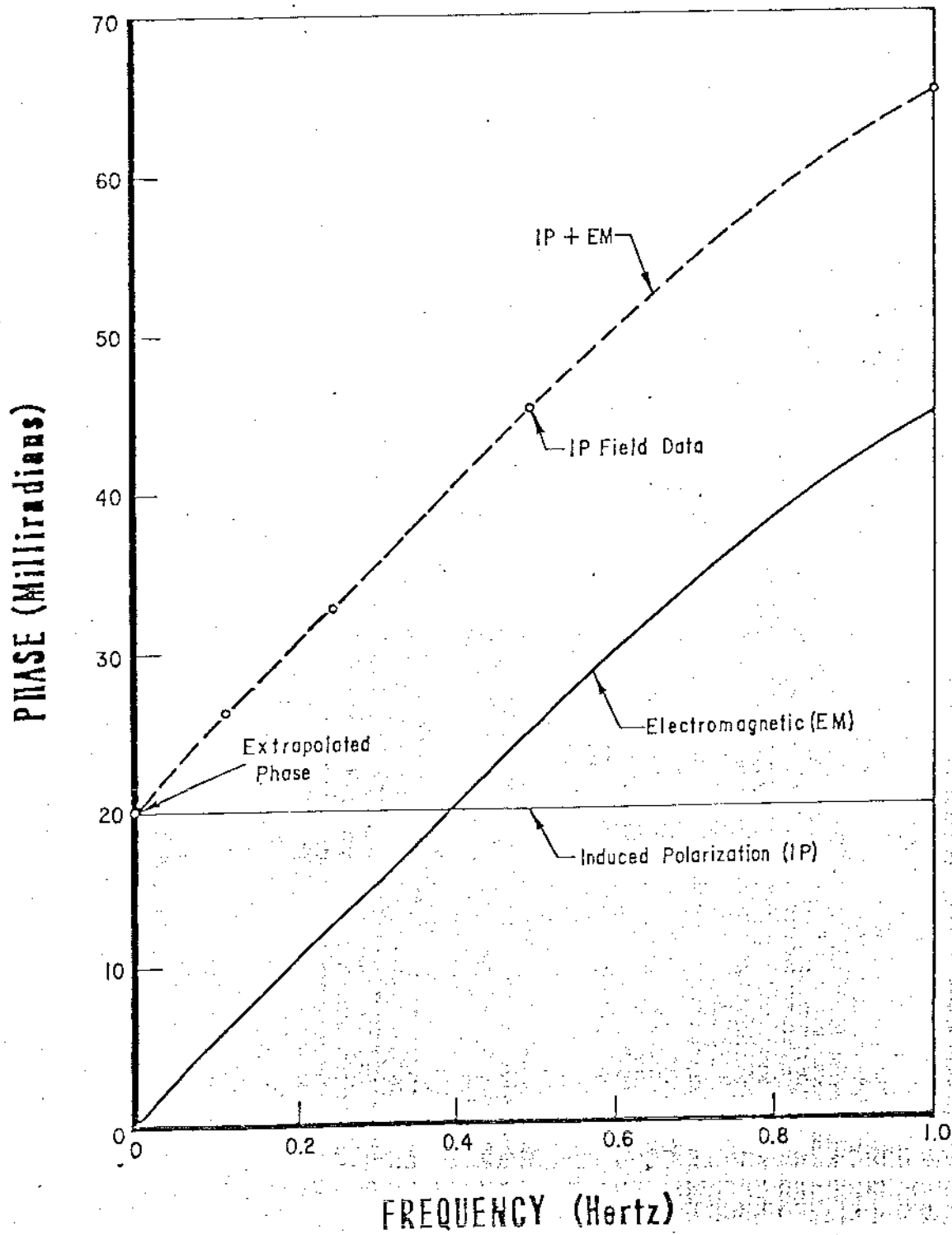
$f = 0.5 \text{ hz}$



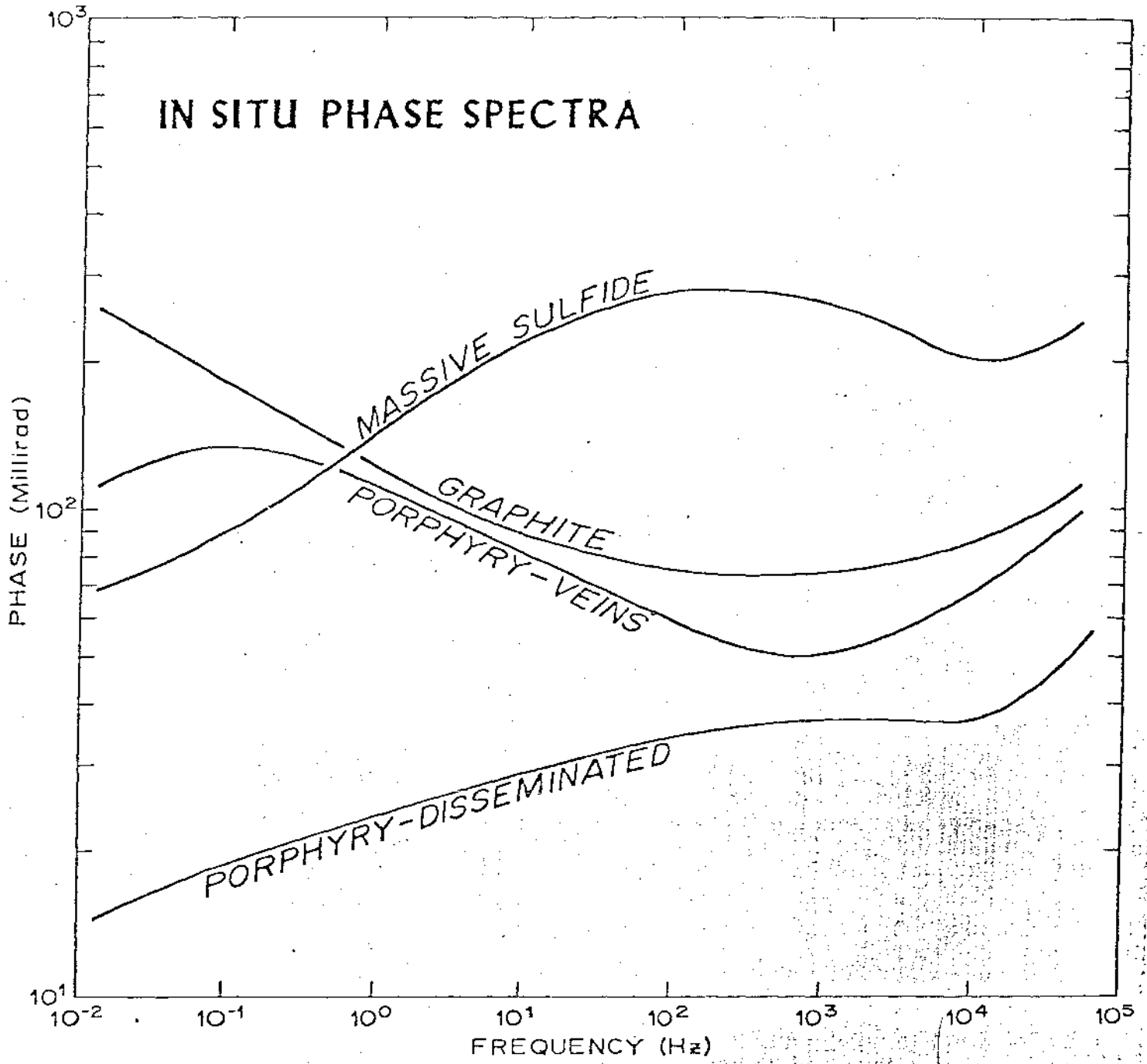
$f = 0.1 \text{ hz}$



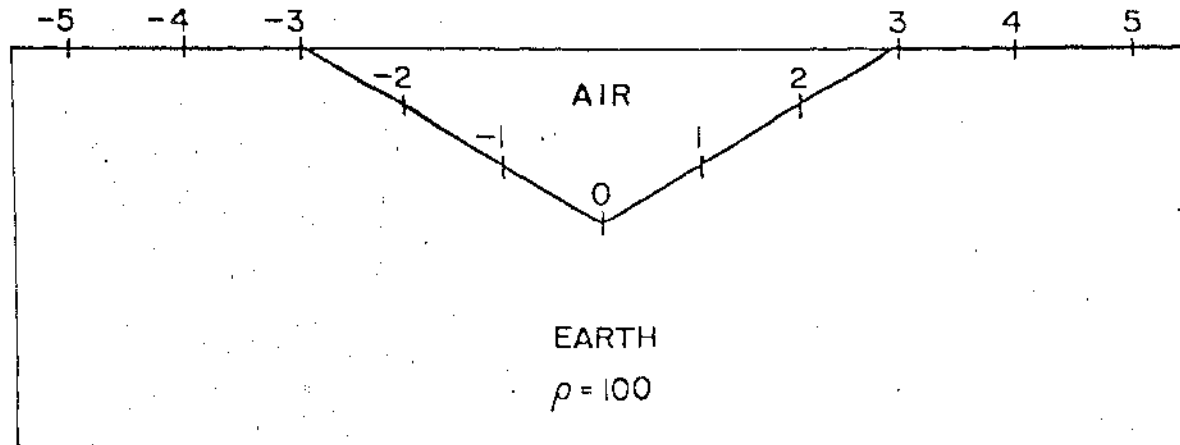
# REMOVING EM COUPLING



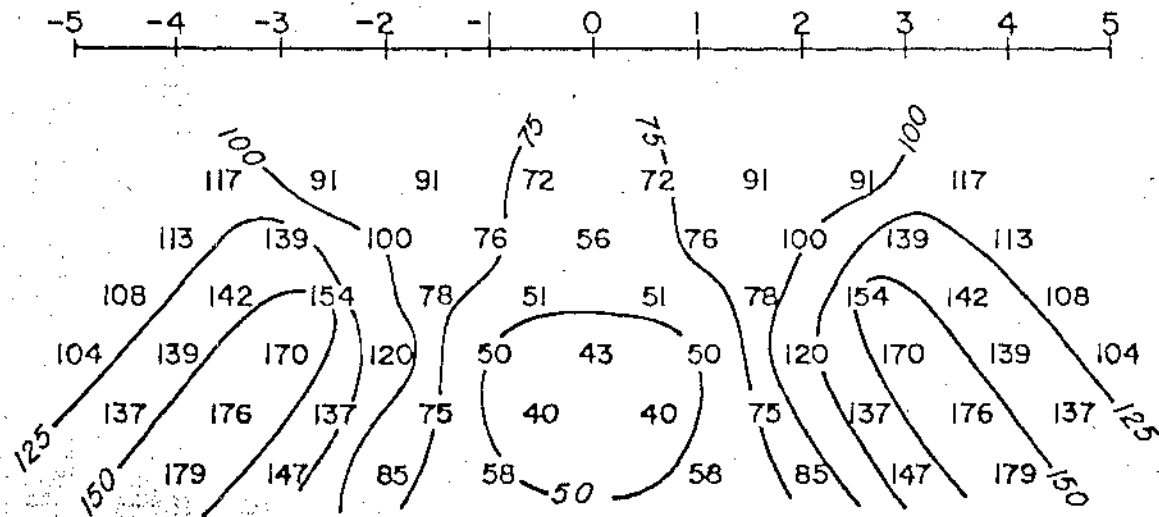
# IN SITU PHASE SPECTRA



# VALLEY RESISTIVITY EFFECT



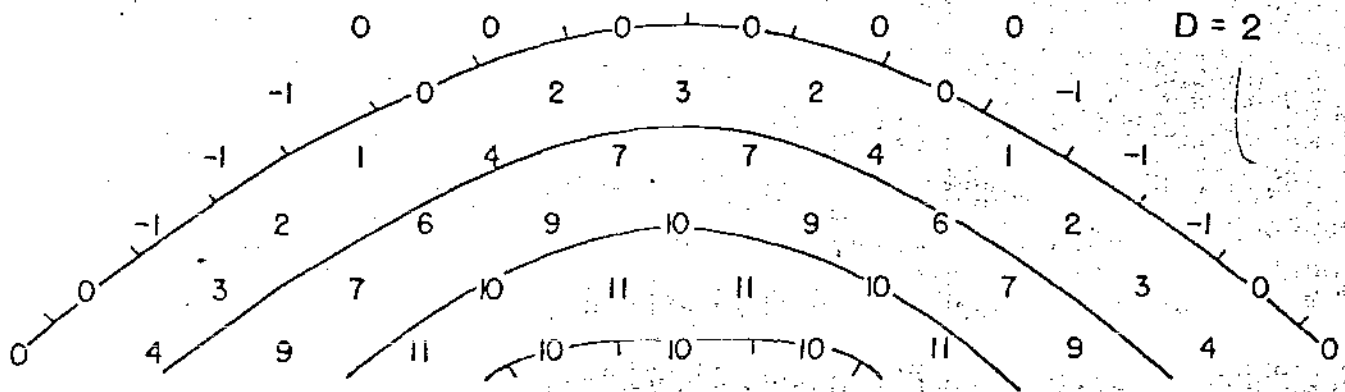
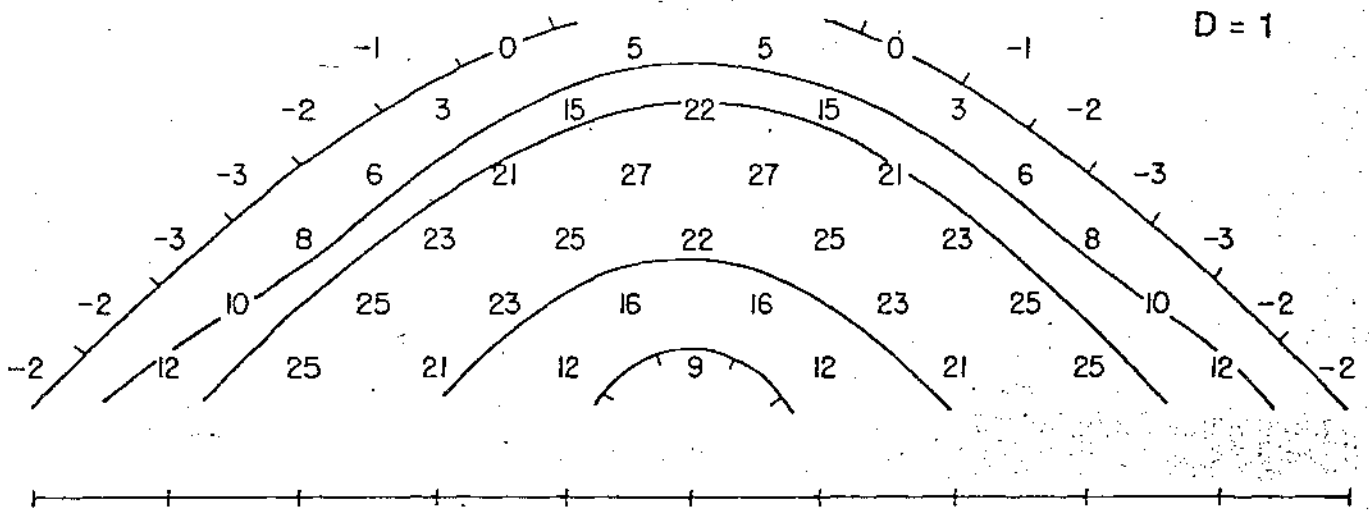
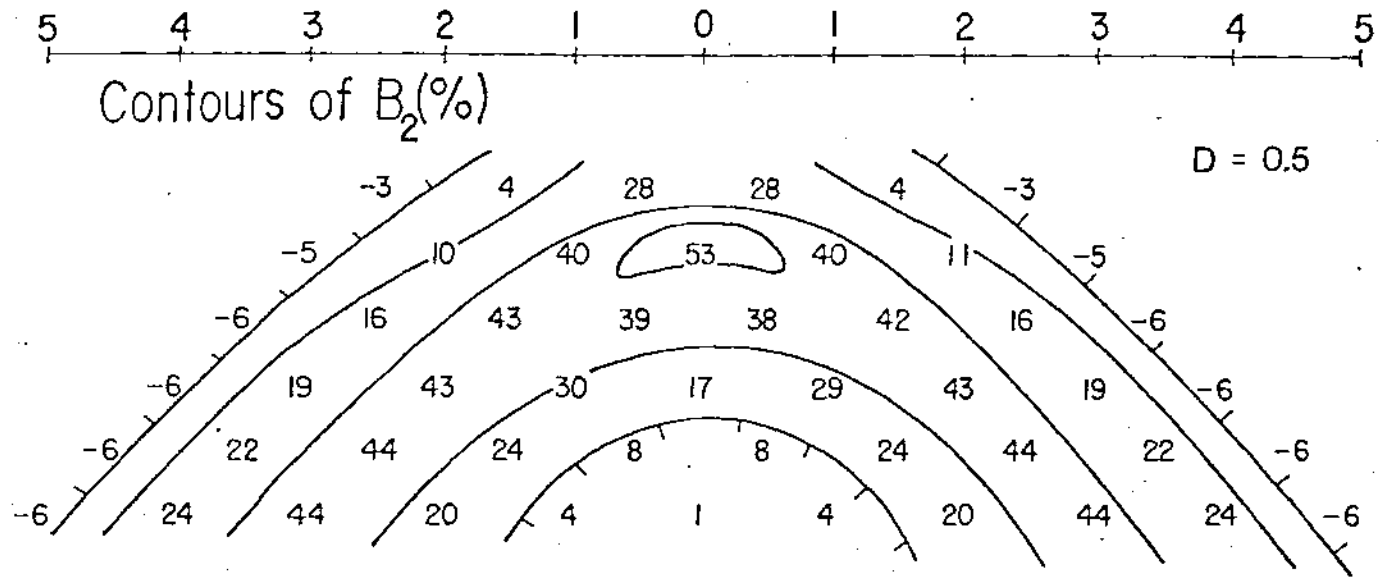
## APPARENT RESISTIVITY



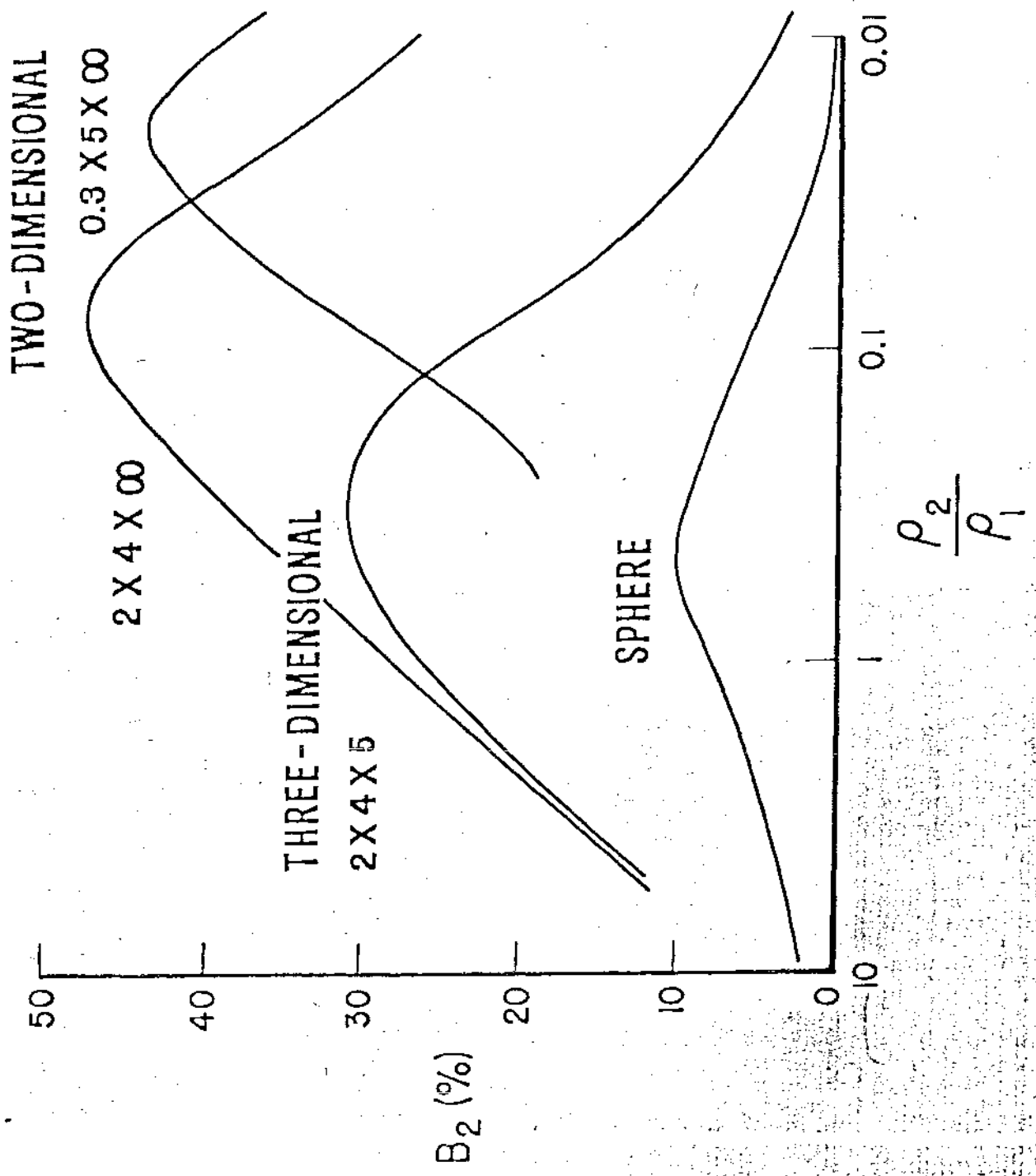




# EFFECT OF DEPTH



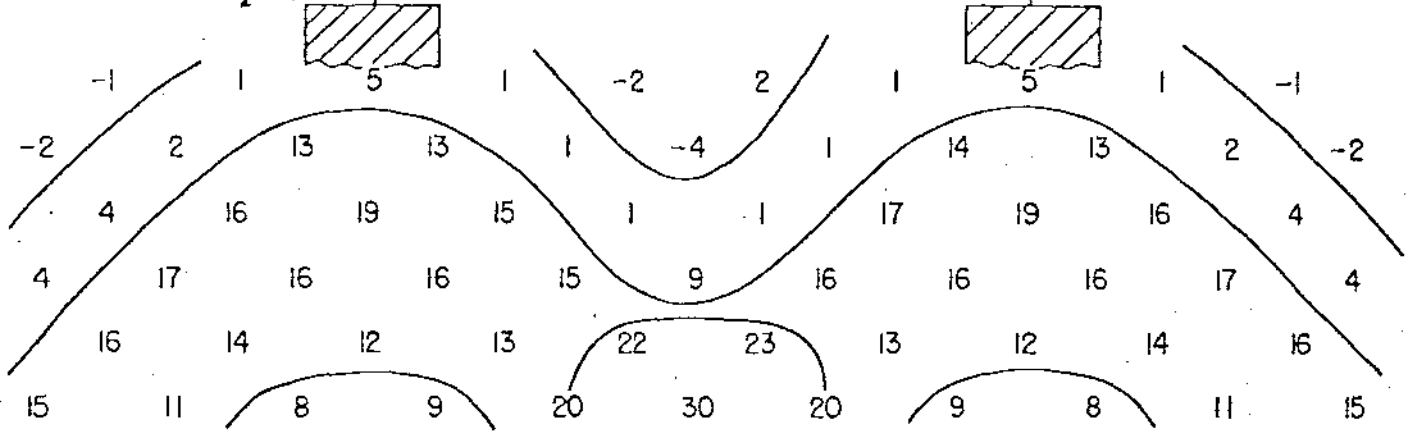
# EFFECT OF RESISTIVITY CONTRAST



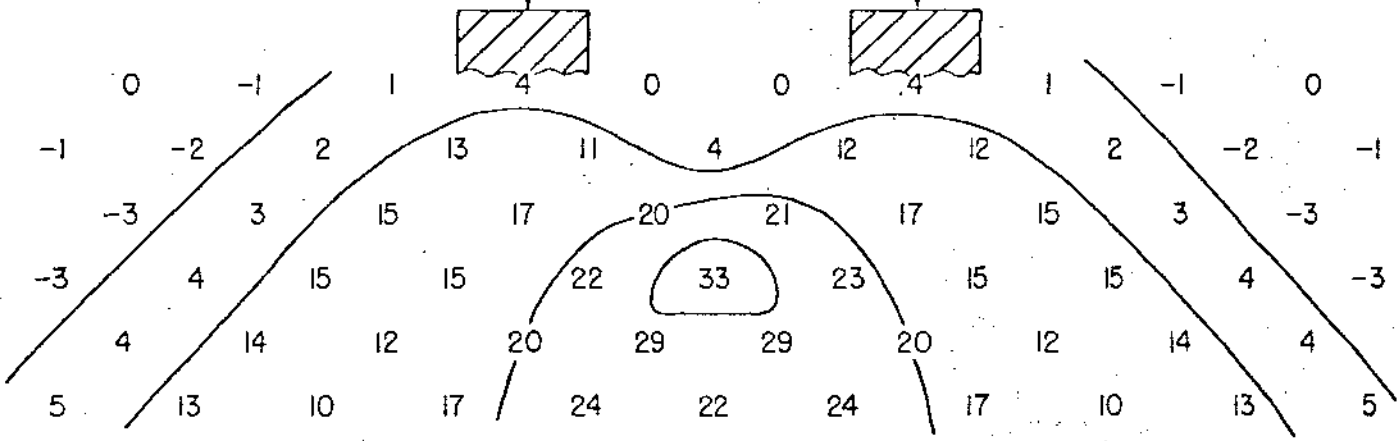
# EFFECT OF MULTIPLE BODIES

5 4 3 2 | 0 | 2 3 4 5

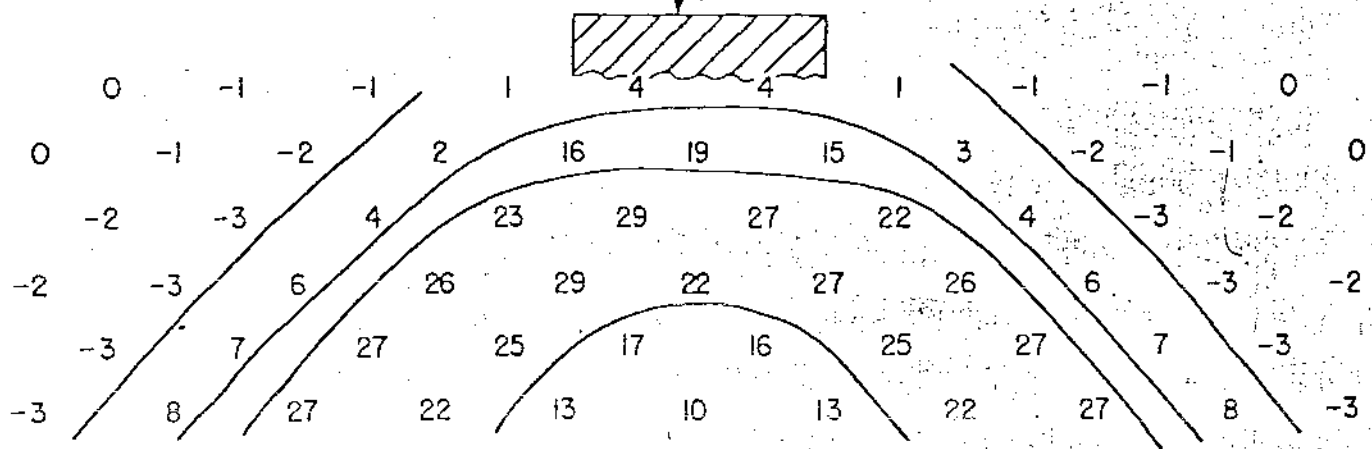
Contours of  $B_2(\%)$



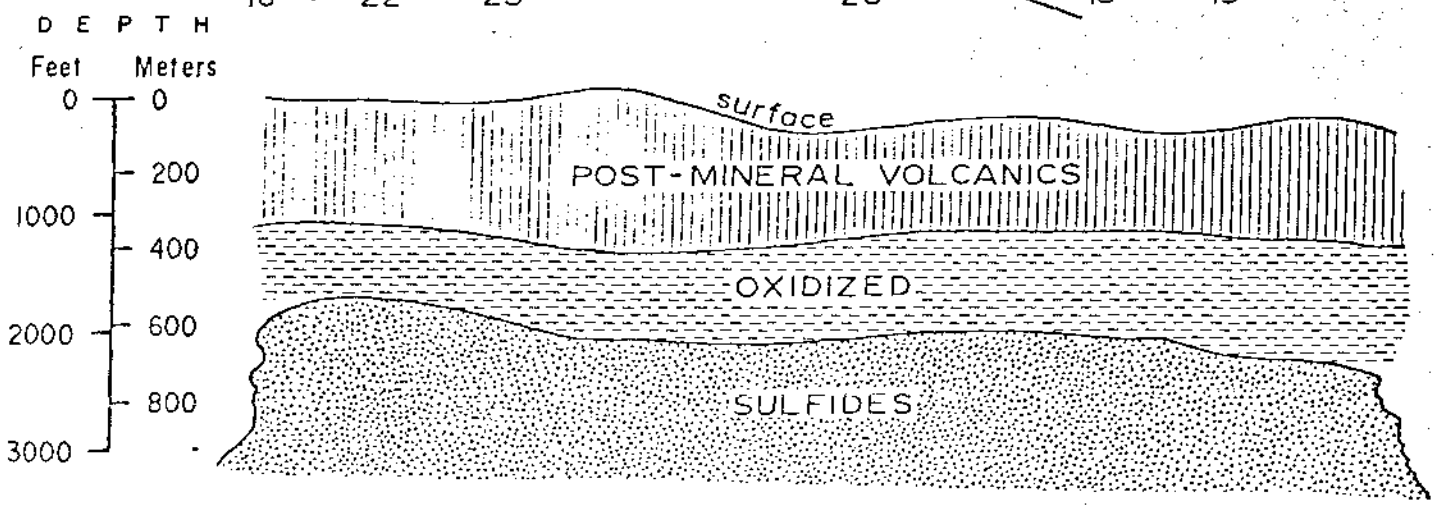
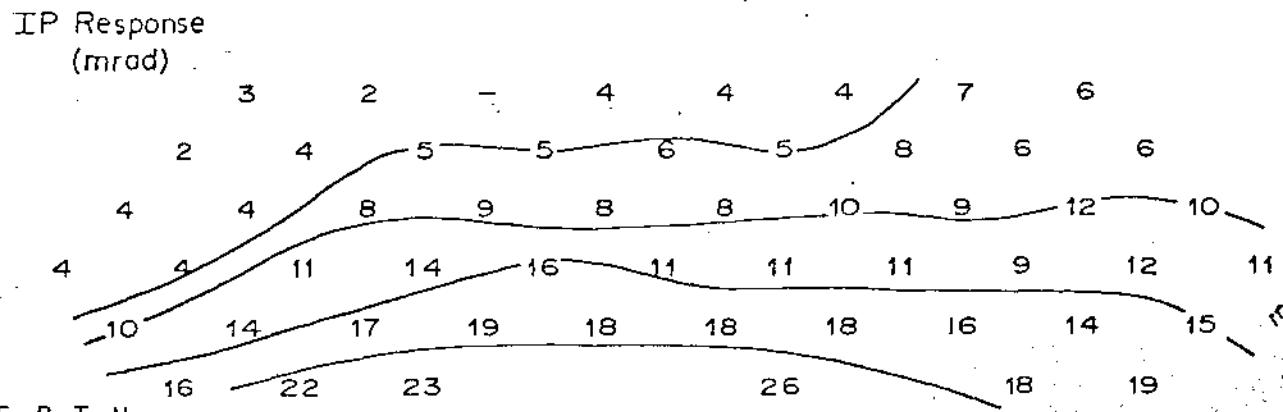
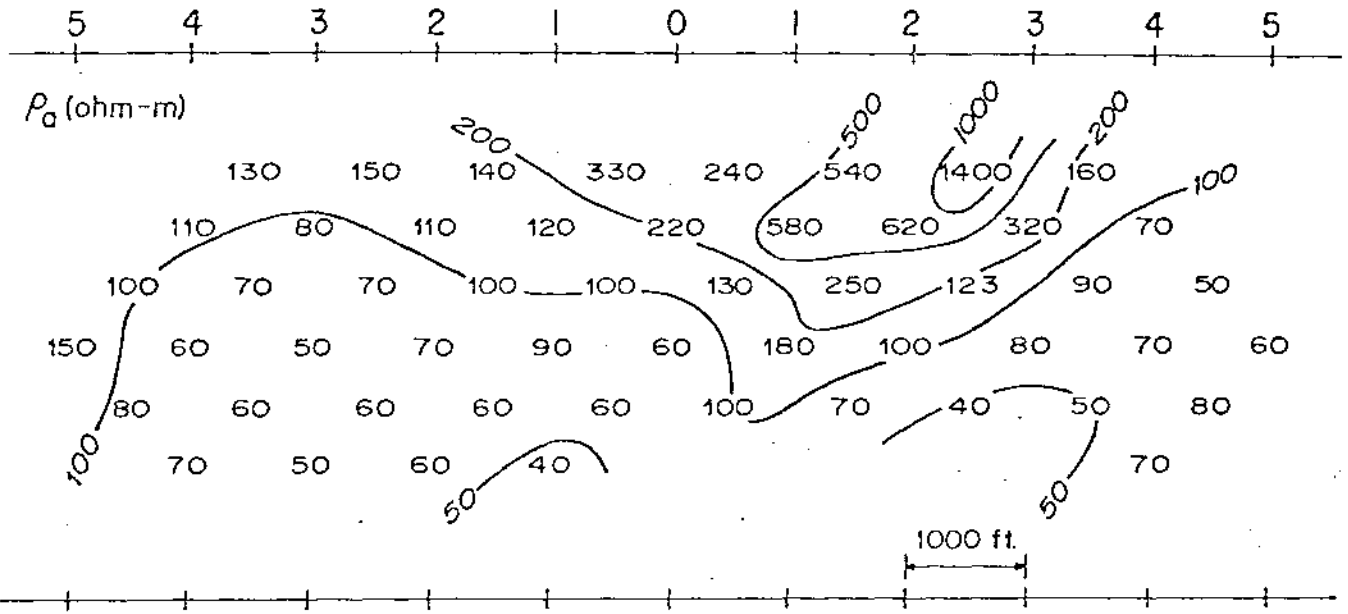
5 4 3 2 | 0 | 2 3 4 5



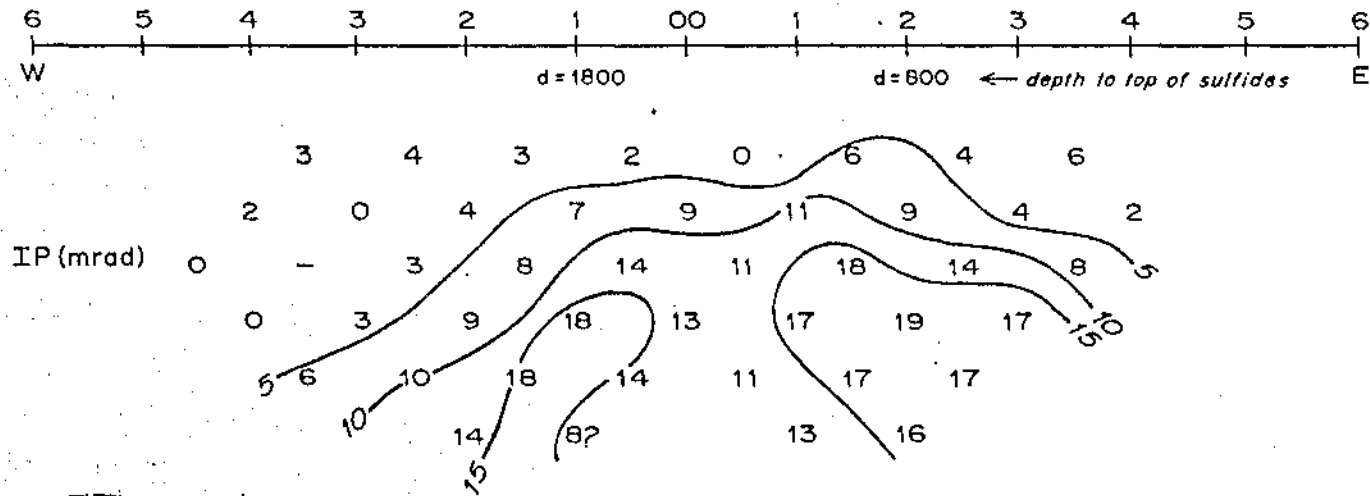
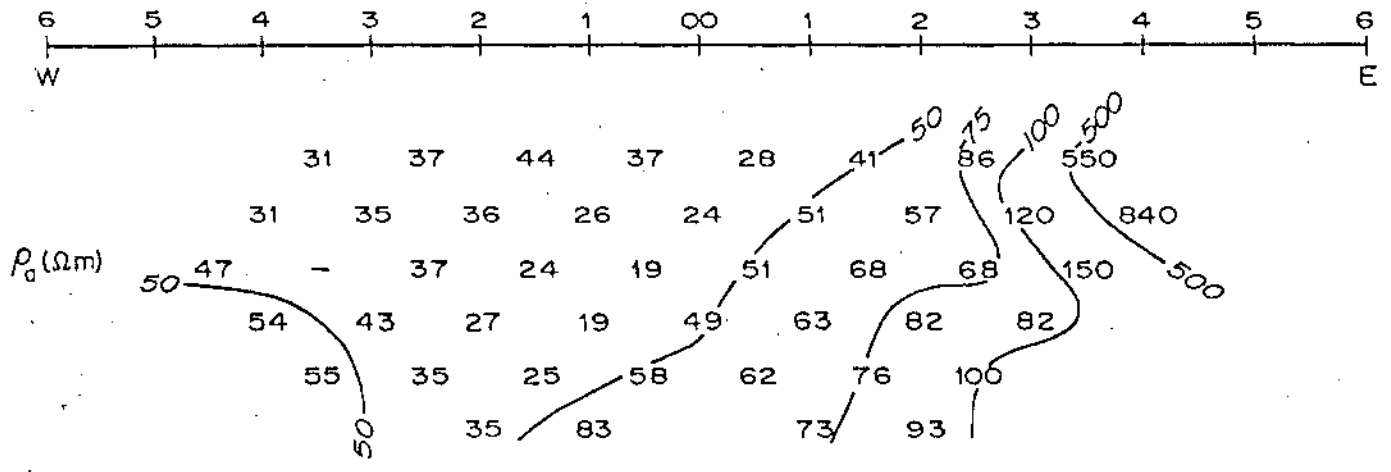
5 4 3 2 | 0 | 2 3 4 5



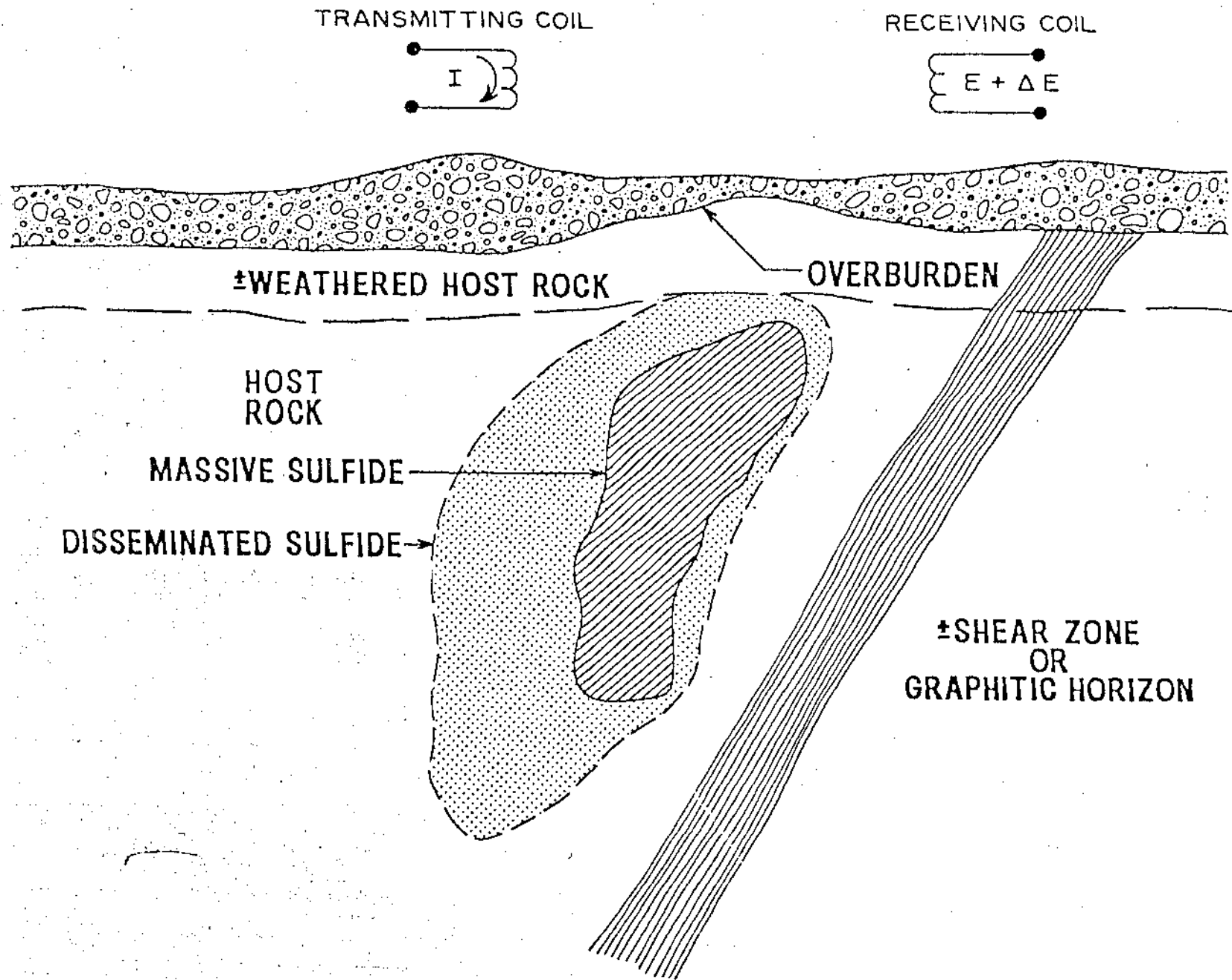
# SAFFORD CASE HISTORY



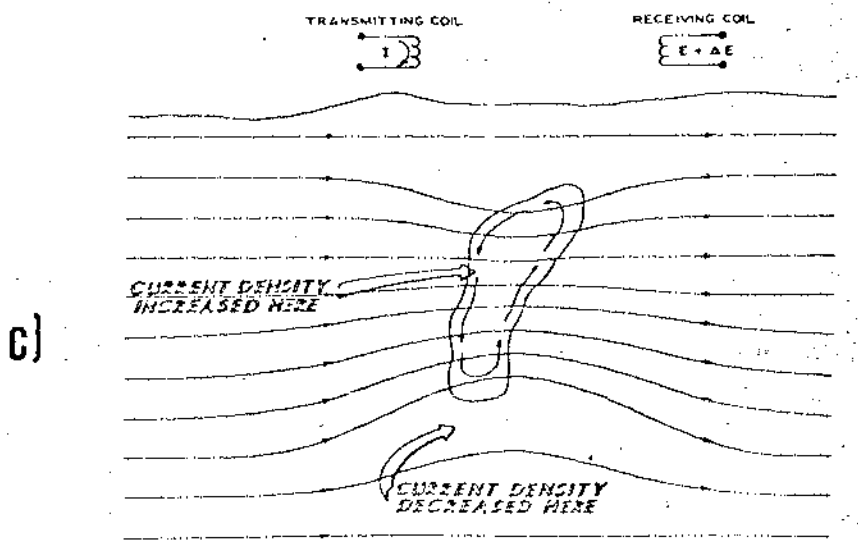
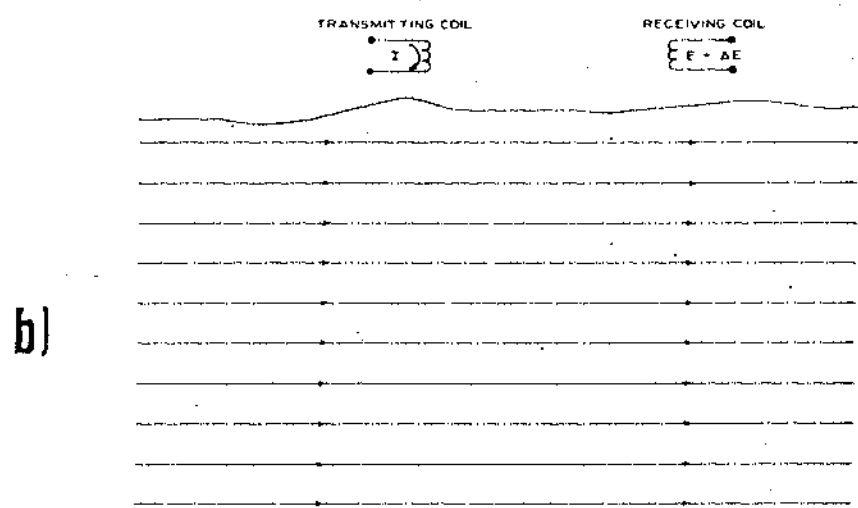
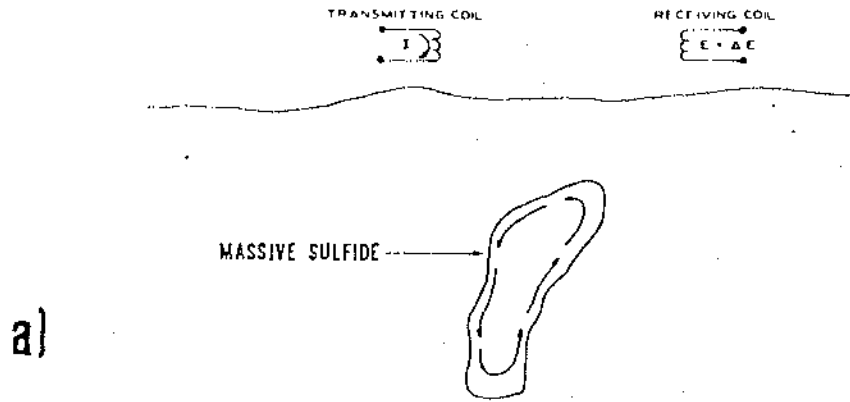
# LAKESHORE CASE HISTORY



# EM SEARCH PROBLEM

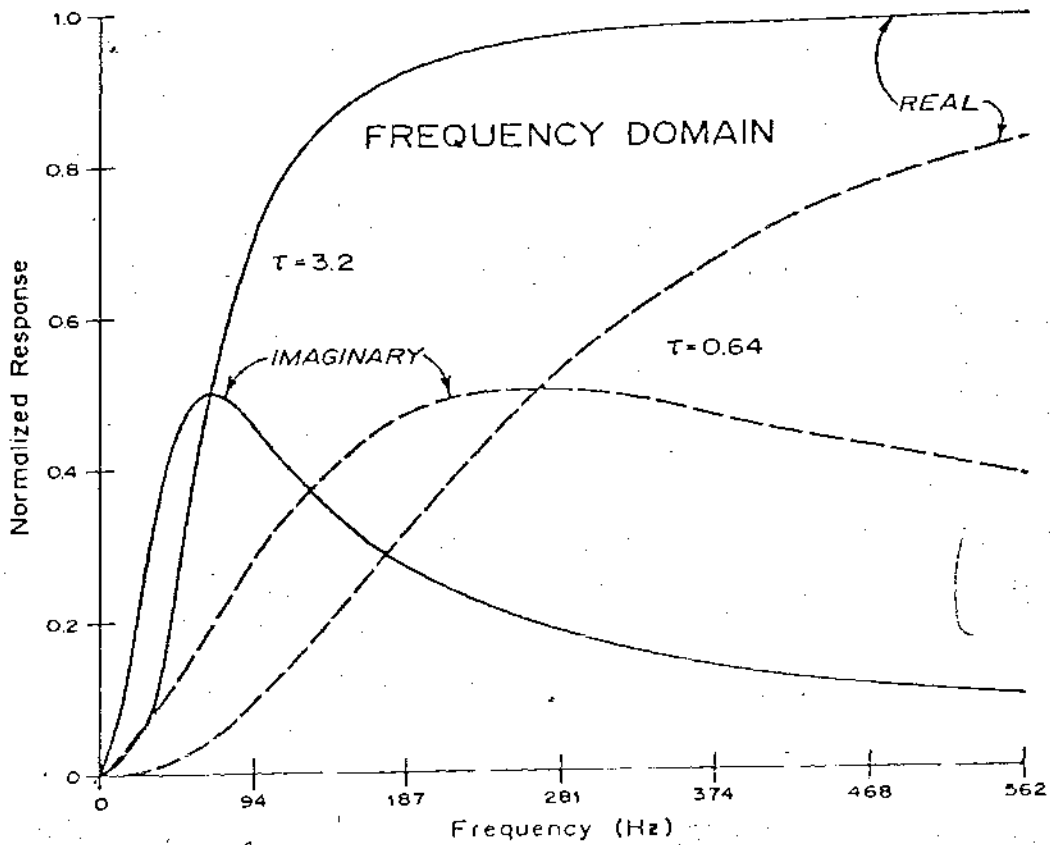
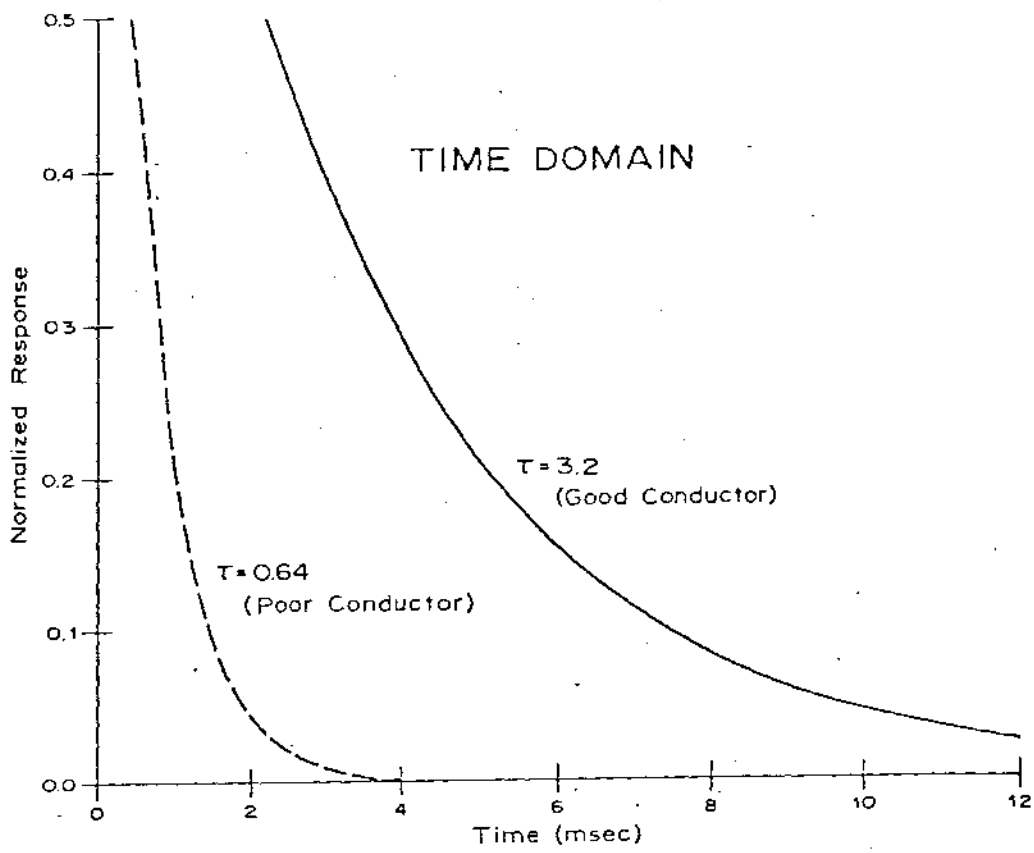


# EM INDUCTION AND CURRENT GATHERING

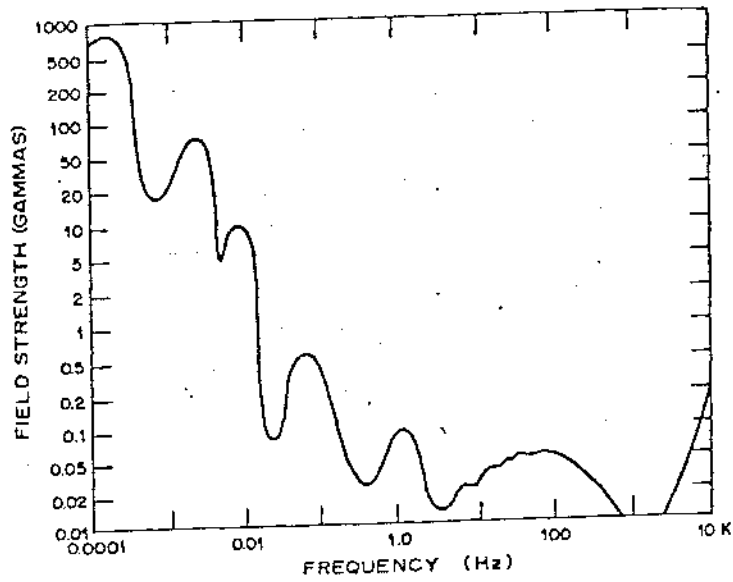




# FEM AND TEM RESPONSES, GOOD AND POOR CONDUCTORS

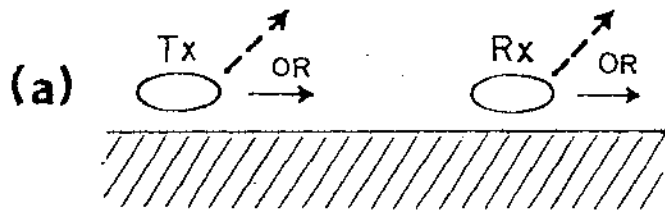


# NATURAL MAGNETIC FIELD SPECTRUM

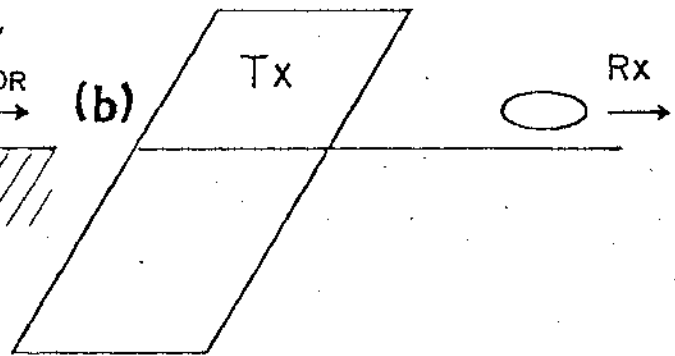


# BASIC GROUND EM METHODS

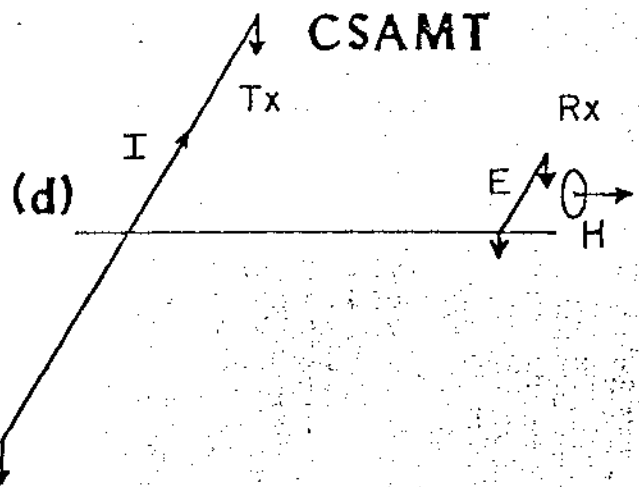
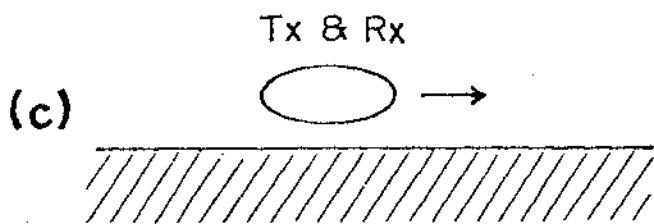
## Two-loop



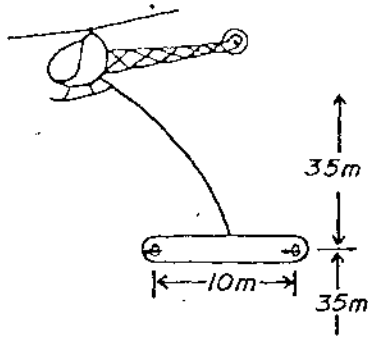
## Large source loop



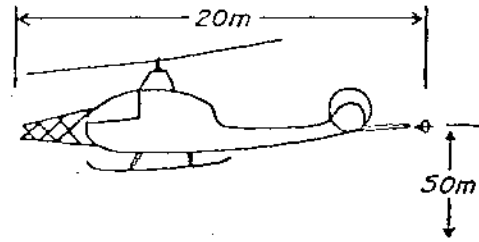
## Single-loop



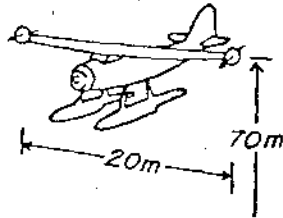
# BASIC AIRBORNE SYSTEMS



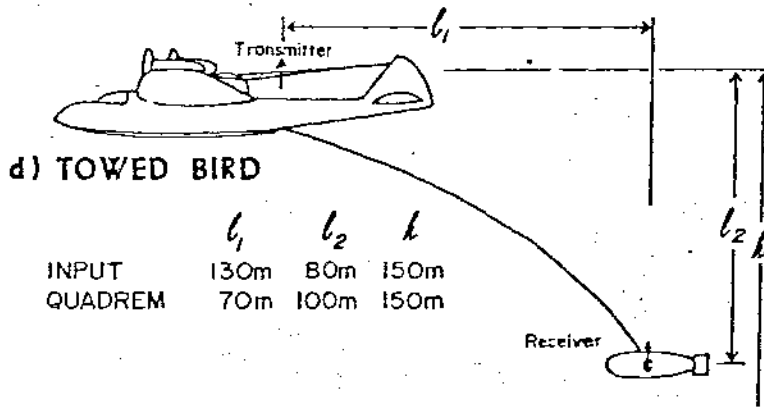
a) HELICOPTER TOWED-BOOM



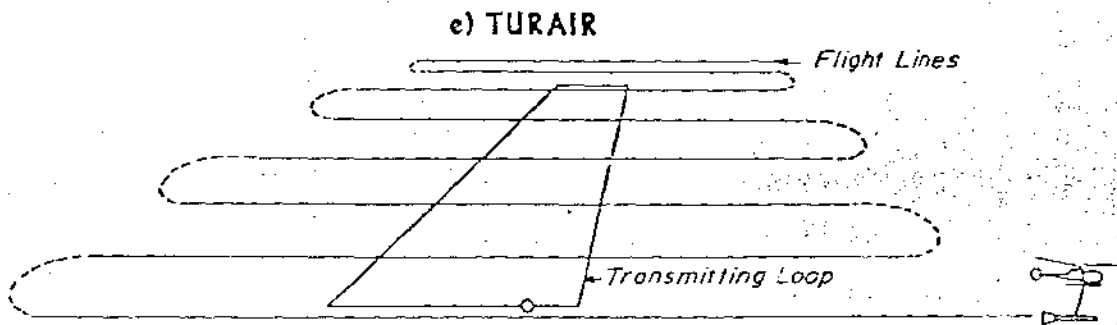
b) HELICOPTER BOOM



c) WING-TIP BOOM

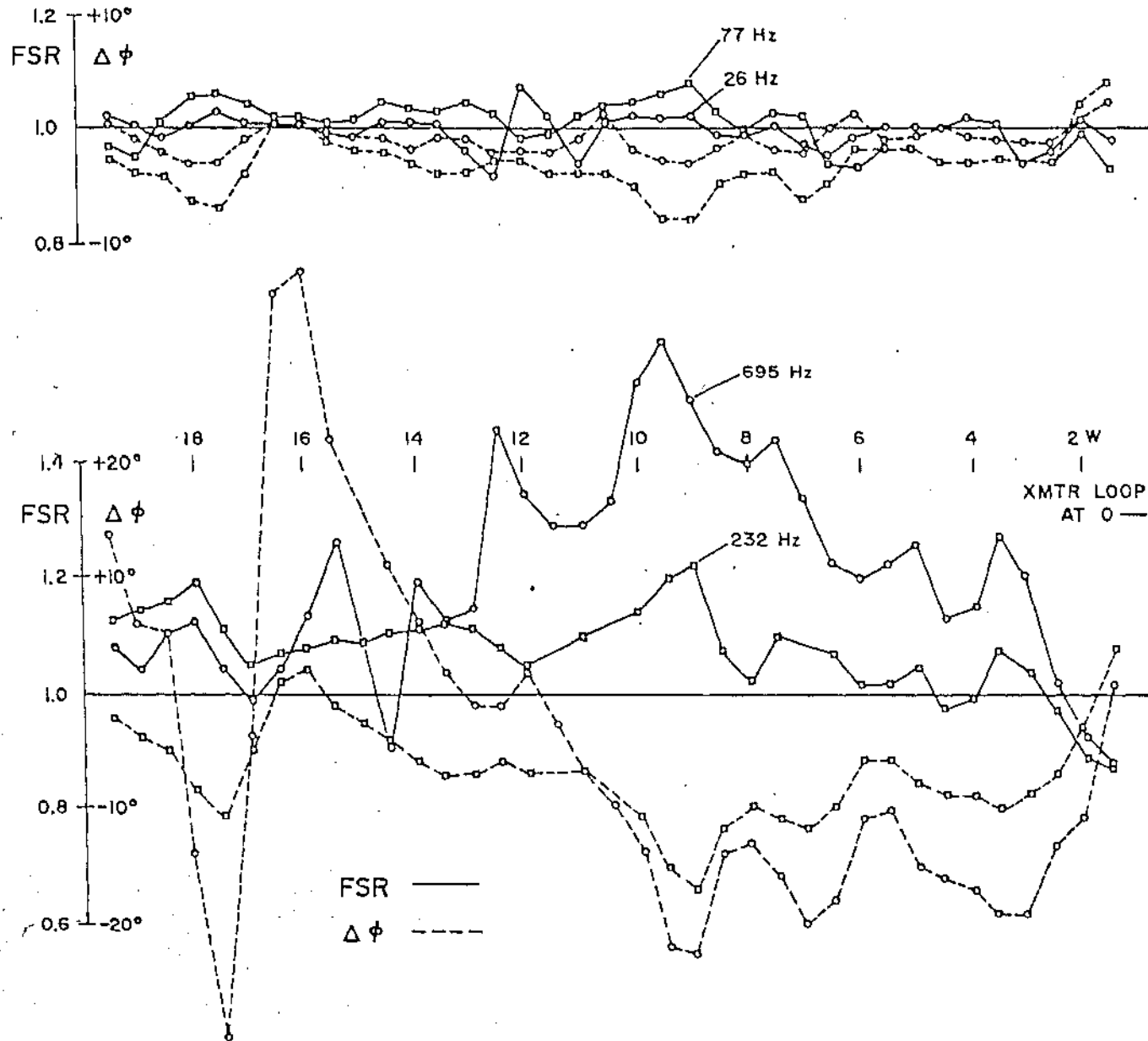


d) TOWED BIRD

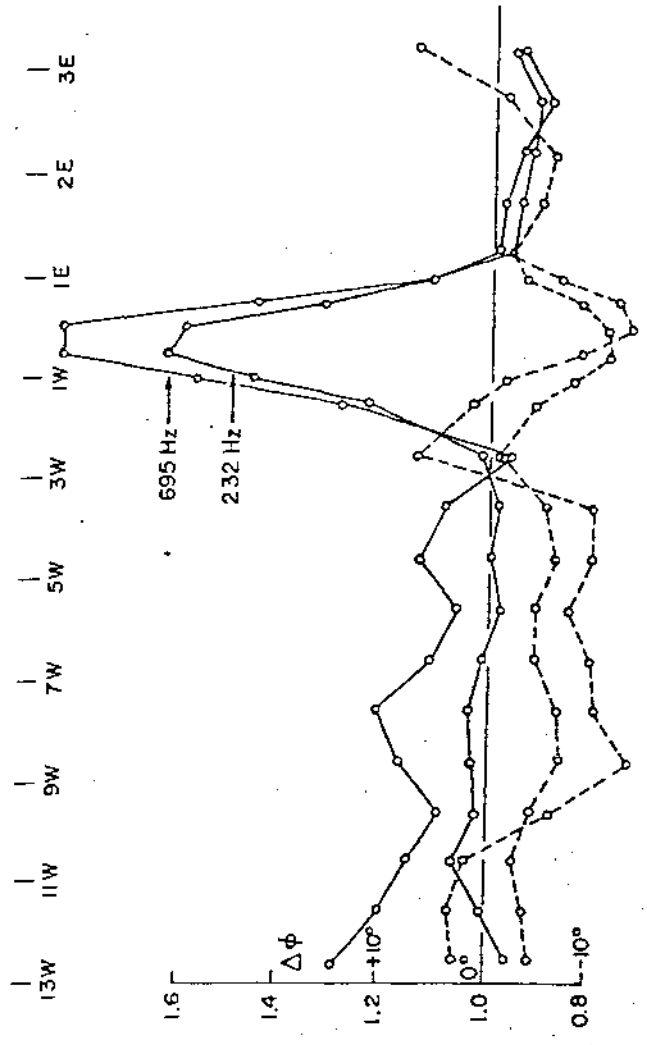
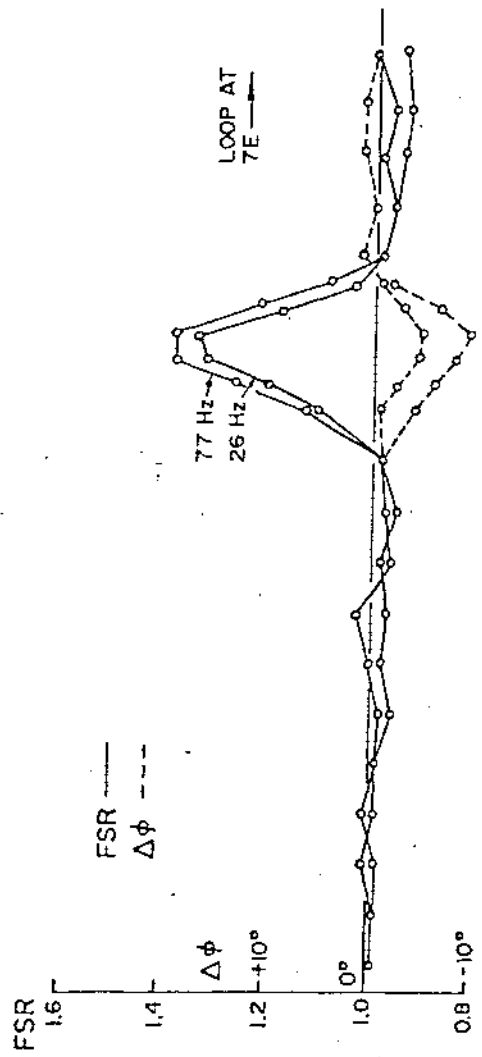


e) TURAIR

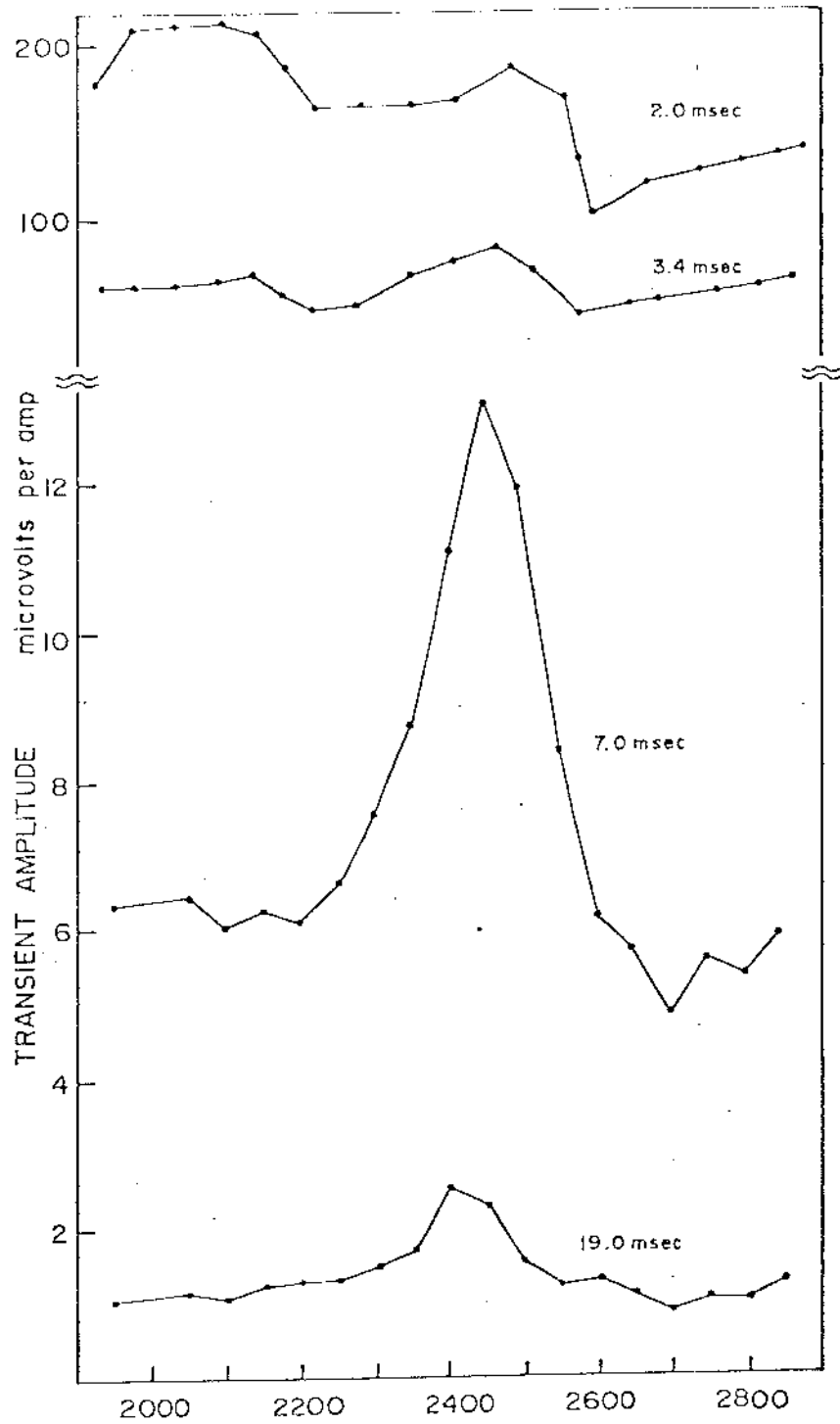
# DEEP WEATHERING CASE HISTORY



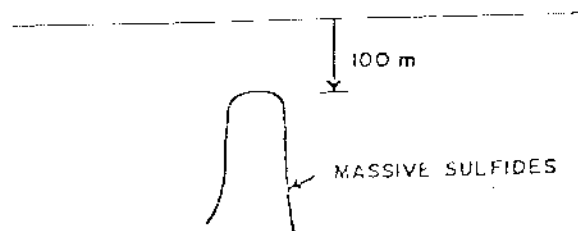
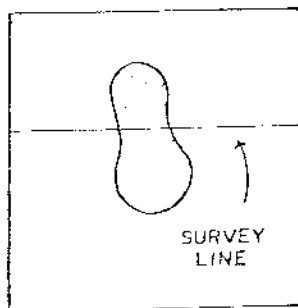
# FREDDIE WELL CASE HISTORY



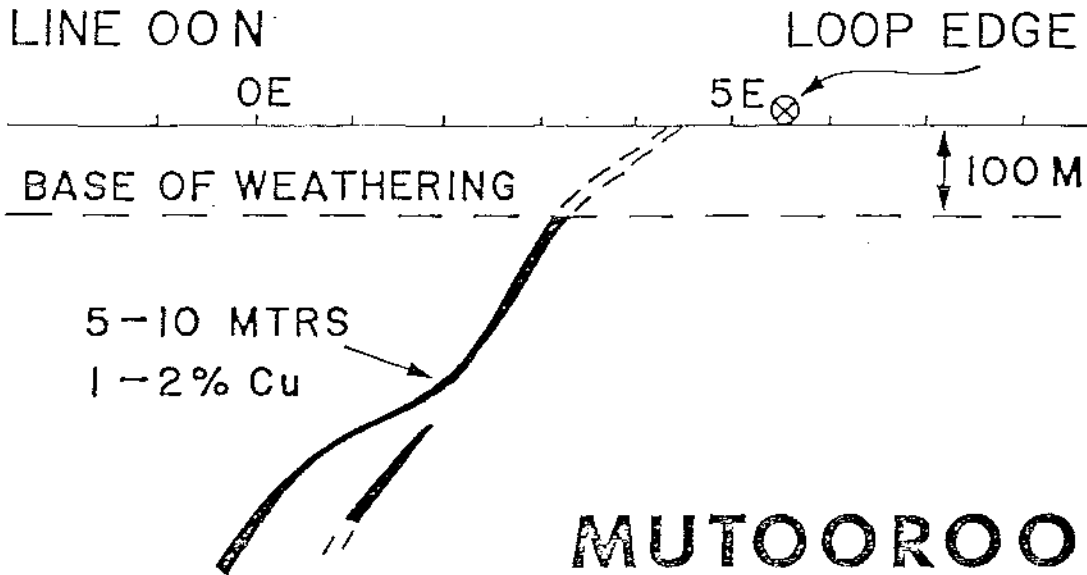
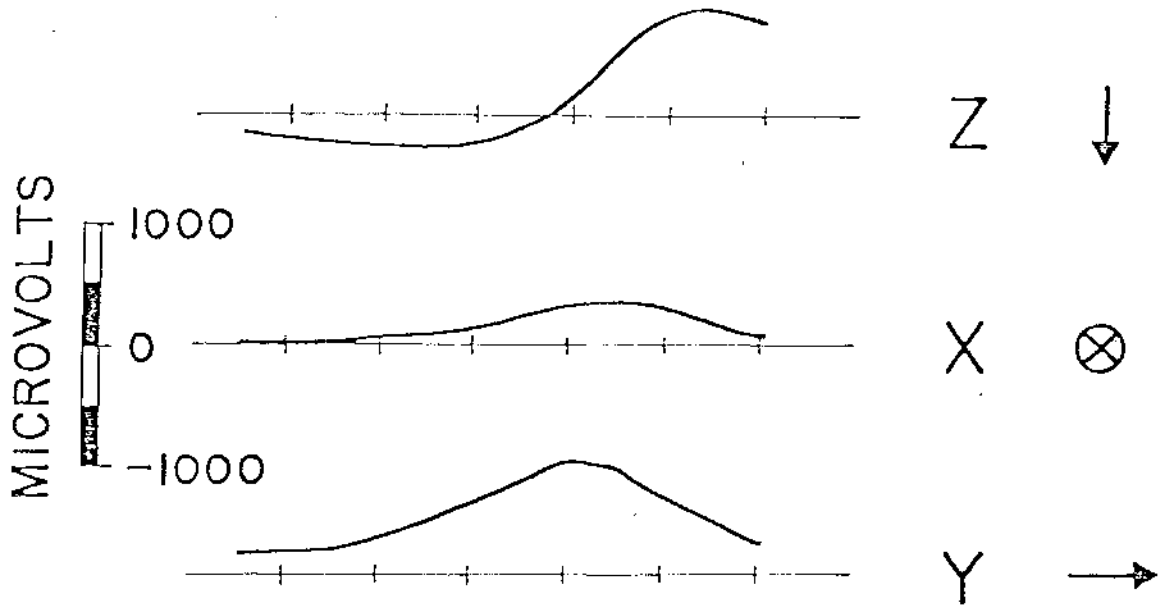
# ELURA DEPOSIT, N.S.W., AUSTRALIA



## PLAN



TIME  
5.63 MSEC



# MUTOOROO EMP SURVEY

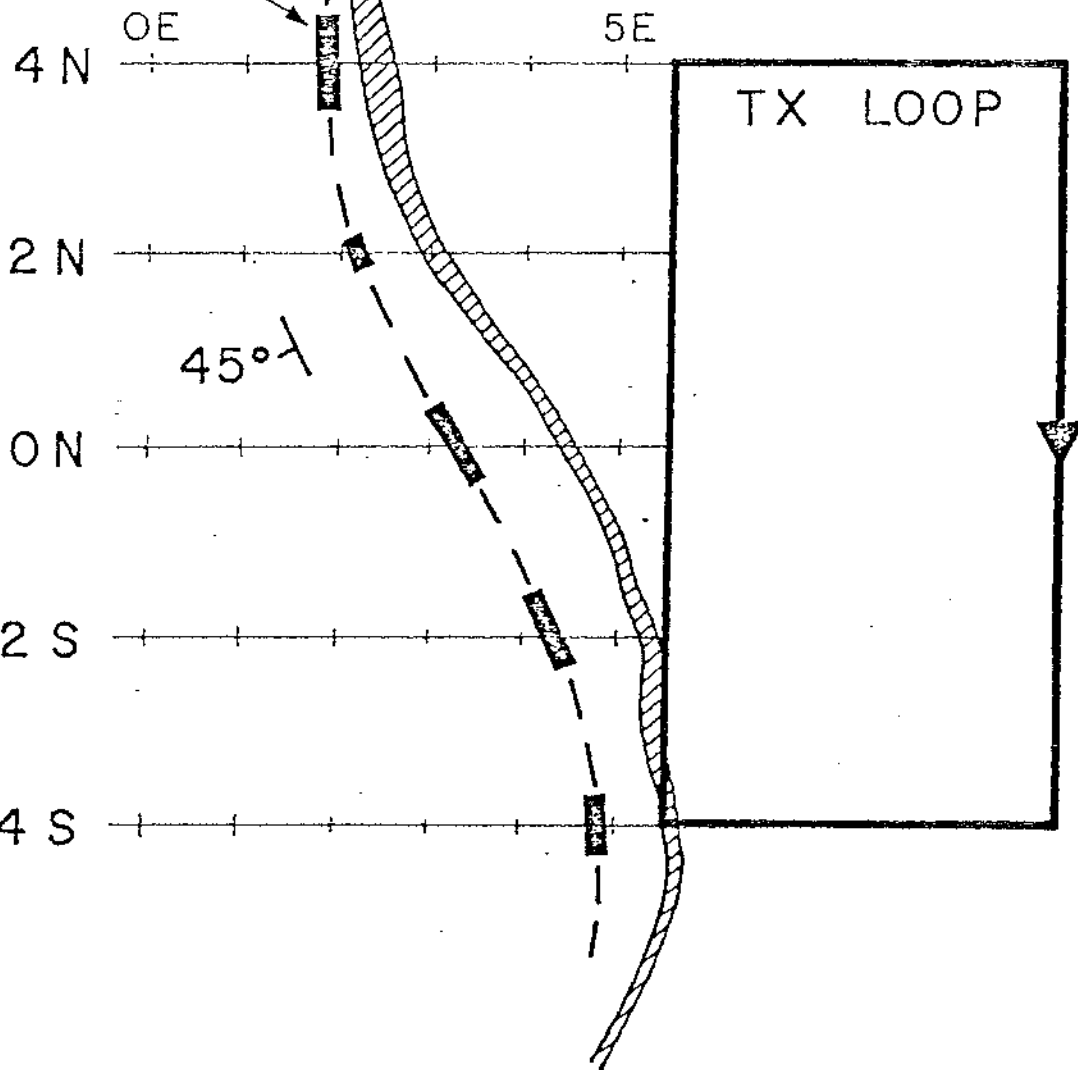
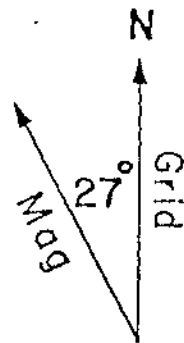
CHANNEL PLOTS





INTERPRETED  
POSITION OF  
CONDUCTOR

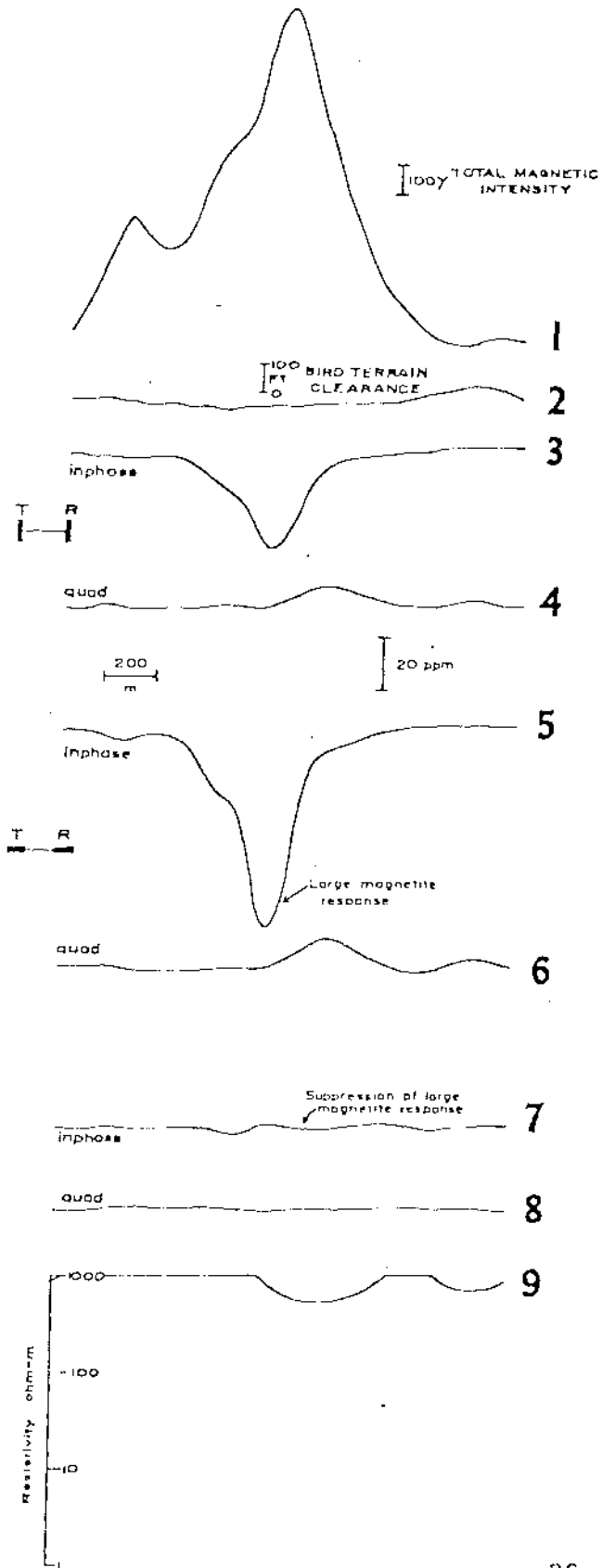
WEATHERED  
OUTCROP  
POSITION



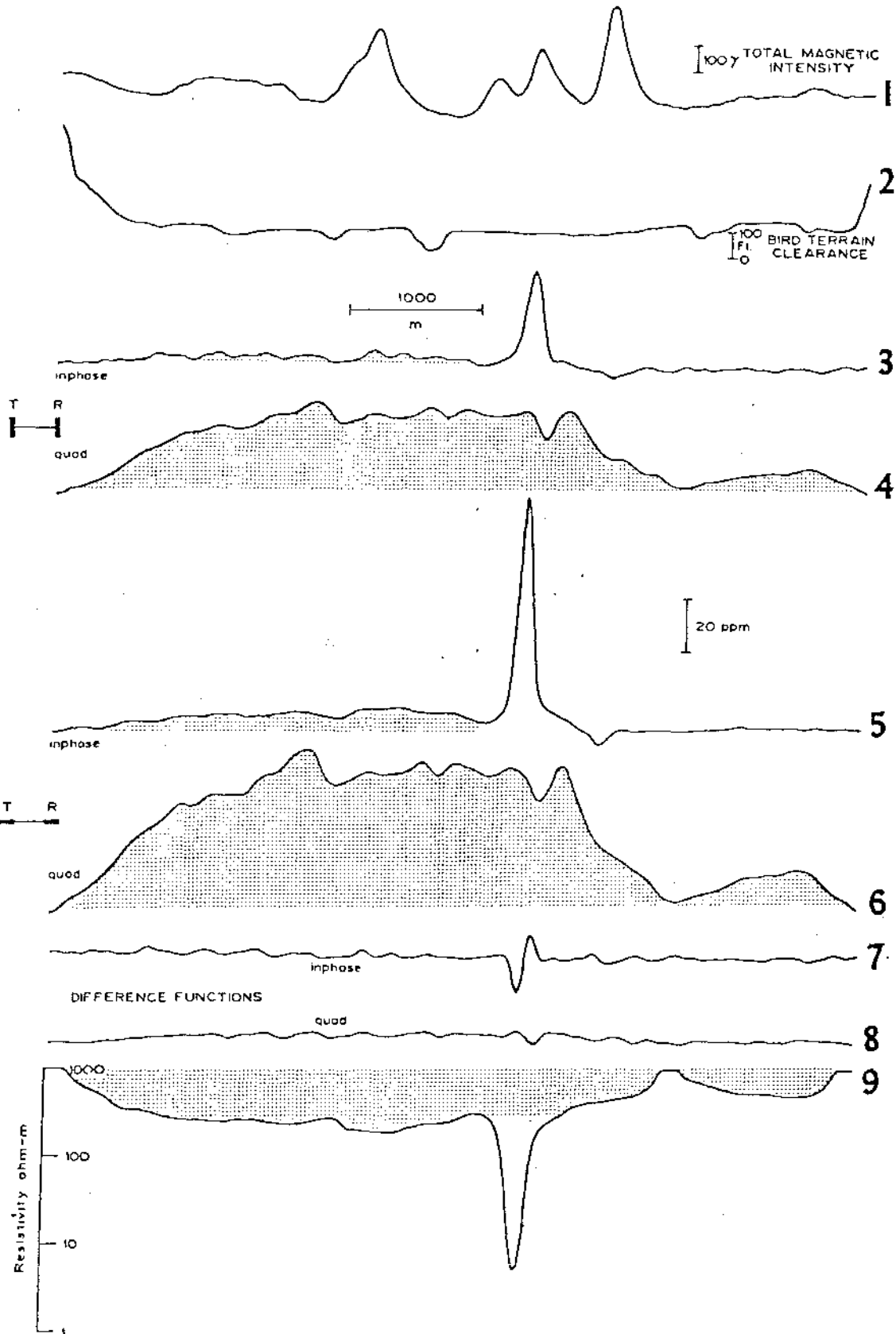
# MUTOOROO EMP SURVEY



# DIGHEM II CASE HISTORY

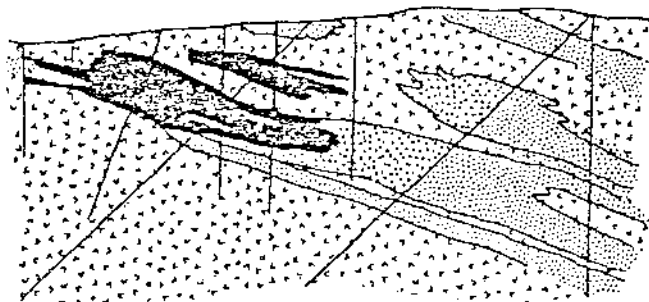
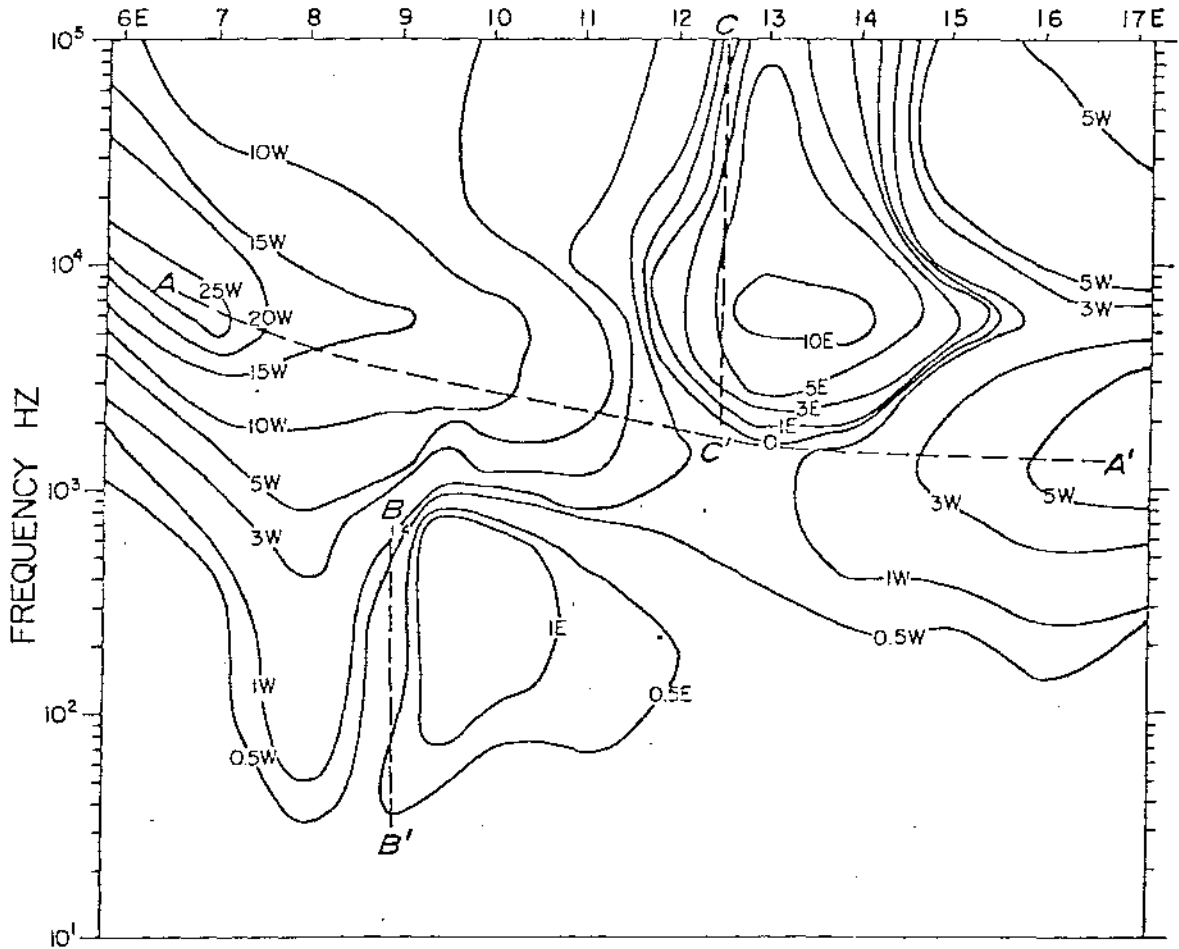



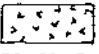

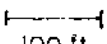
# DIGHEM II CASE HISTORY



# 14 FREQUENCY CASE HISTORY

LINE 20  
 VERTICAL AXIAL COIL  
 TILT ANGLE-DEGREES  
 NORMALIZED TO 10.5 HZ  
 Tx 3+00E



-  MASSIVE SULFIDES
-  INTERMEDIATE TO BASIC VOLCANICS
-  FELSIC TUFF (PYRITIC)
-  100 ft.

# INPUT CASE HISTORY

